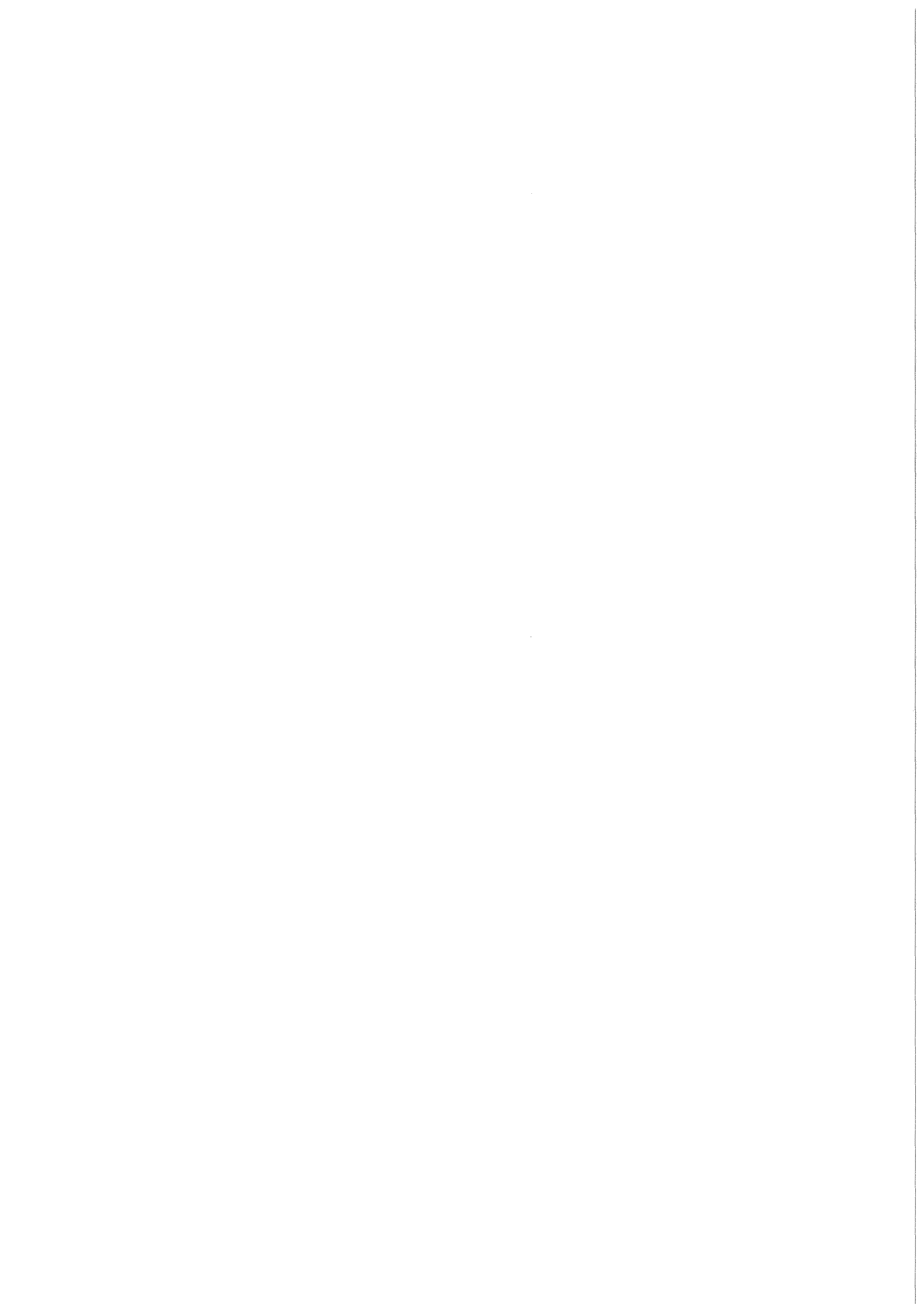


KfK 3276
März 1982

Vapor Pressures of Oxide Reactor Fuels above 3000 K: Review and Perspective

W. Breitung
Institut für Neutronenphysik und Reaktortechnik
Projekt Schneller Brüter

Kernforschungszentrum Karlsruhe



KERNFORSCHUNGSZENTRUM KARLSRUHE

Institut für Neutronenphysik und Reaktortechnik

Projekt Schneller Brüter

KfK 3276

Vapor Pressures of Oxide Reactor Fuels above 3000 K:

Review and Perspective

W. Breitung

Kernforschungszentrum Karlsruhe GmbH, Karlsruhe

Als Manuskript vervielfältigt
Für diesen Bericht behalten wir uns alle Rechte vor

Kernforschungszentrum Karlsruhe GmbH
ISSN 0303-4003

Vapor Pressures of Oxide Reactor Fuels above 3000 K:

Review and Perspective

ABSTRACT

Vapor pressures of liquid oxide reactor fuels are among the most important material data required for theoretical analyses of Hypothetical Core Disruptive Accidents in Fast Breeder Reactors. This report is an attempt to completely summarize and critically review the numerous theoretical and experimental results published for the pressure-temperature and pressure-energy relation of un-irradiated UO_2 and $(\text{U,Pu})\text{O}_2$. First - to define the research goal - the precision in the saturation vapor pressure is quantified which is required for the purpose of HCDA calculations. Then the various theoretical and experimental methods used for the determination of p-T and p-U data are reviewed with respect to their principles, results and uncertainties. The achievements of the individual methods are discussed in the light of the research goal and - in view of the widely scattered data - recommendations are made concerning the p-T and p-U relation of UO_2 . Finally, the most important future research areas are identified, including some specific research proposals which aim at reducing the still large uncertainties in fuel vapor pressures down to the desired level.

Dampfdrücke von oxidischen Kernbrennstoffen oberhalb 3000 K:

Übersicht und Ausblick

ZUSAMMENFASSUNG

Dampfdruckdaten für die flüssige Phase von Reaktorbrennstoffen gehören zu den wichtigsten Materialdaten für die theoretische Analyse von hypothetischen Störfällen bei Schnellen Brütern. In diesem Bericht wird versucht, die zahlreichen theoretischen und experimentellen Ergebnisse, die für den Dampfdruck-Temperatur- und den Dampfdruck-Energie-Zusammenhang von unbestrahltem UO_2 und $(\text{U,Pu})\text{O}_2$ veröffentlicht wurden, zusammenzufassen und kritisch zu sichten. Als erstes wird - um das Ziel der Untersuchung einzugrenzen - festgelegt, welche Genauigkeit bei den Werten des Sättigungsdampfdrucks für die Analyse hypothetischer Störfälle erforderlich ist. Sodann wird ein Überblick über die verschiedenen theoretischen und experimentellen Methoden, die bei der Bestimmung der p-T- und der p-U-Daten angewandt wurden, gegeben. Hierin eingeschlossen sind Darstellungen der Ergebnisse und der Unsicherheiten. Die Leistungsfähigkeit der verschiedenen Methoden wird im Hinblick auf das o.g. Ziel der Untersuchungen diskutiert und es werden - angesichts der breiten Streuung der Daten - Empfehlungen für die p-T- und p-U-Beziehungen von UO_2 gegeben. Schließlich werden die wichtigsten künftigen Arbeitsziele identifiziert und es werden Vorschläge für Forschungsarbeiten gemacht, die helfen sollen, die noch bestehenden Unsicherheiten bei Brennstoffdampfdruckdaten auf das gewünschte Maß zu reduzieren.

Table of Contents

	<u>Page</u>
Abstract	
1. Introduction	1
2. Definition of Research Goal	3
3. Review of Theoretical Methods	10
3.1 Corresponding States Theory	10
3.1.1 Outline of Theory	10
3.1.2 Applications	12
3.1.3 Evaluation of Method	14
3.2 Significant Structure Theory	15
3.2.1 Outline of Theory	15
3.2.2 Applications	16
3.2.3 Evaluation of Method	17
3.3 Law of Mass Action	19
3.3.1 Outline of Theory	19
3.3.2 Applications	20
3.3.3 Evaluation of Method	22
3.4 Clapeyron - Equation	22
3.4.1 Outline of Theory	22
3.4.2 Applications	23
3.4.3 Evaluation of Method	23
3.5 Assessment of Theoretical p(T) Results	24
3.5.1 Corresponding States Theory	25
3.5.2 Significant Structure Theory	26
3.5.3 Law of Mass Action	27
3.5.4 Clapeyron-Equation	27
3.5.5 Summary	28
4. Review of Experimental Methods	29
4.1 ANL Transpiration Technique	29
4.2 Laser Surface Heating	33
4.2.1 KfK-INR Technique	33
4.2.2 LBL-NASA Technique	39
4.2.3 ITU Technique	42
4.2.3.1 Vacuum Evaporation	42
4.2.3.2 Modified Mach Disk Method	48
4.2.4 MAP Technique	52
4.3 Assessment of Experimental p(T) Results	52
4.3.1 Transpiration Technique	53
4.3.2 KfK-INR Technique	53
4.3.3 LBL-NASA Technique	54
4.3.4 ITU Vacuum Evaporation	55
4.3.5 ITU Mach Disk Method	55
4.3.6 Open Questions in Laser Evaporation	56
4.3.6.1 Optical Absorption in UO ₂ Vapor	56
4.3.6.2 Composition Changes in the Evaporating Surface	58

4.3.6.3	Laser Induced Evaporation	59
4.3.7	Summary	60
4.4	Fission Heating	61
4.4.1	SNL Technique	61
4.4.2	CEA Technique	71
4.4.3	Integral Pin Tests	76
4.5	Electron Beam Heating	77
4.6	Assessment of p(U) Results	83
4.6.1	Theoretical Work	83
4.6.2	Experimental Work	84
4.6.3	Summary	86
5.	Results for (U,Pu) Mixed Oxides	88
5.1	Theoretical Results	88
5.2	Experimental Results	89
5.2.1	ITU Vacuum Evaporation	89
5.2.2	VIPER Experiments	91
5.2.3	SPR III Experiments	92
6.	Future Research Needs	94
6.1	Theoretical Methods	94
6.2	Experimental Methods	96
6.2.1	Laser Surface Heating	96
6.2.2	Fission Heating	98
7.	Summary	99
	References	103
	Appendix I: Viewgraph-Summary	112

1. INTRODUCTION

In a number of countries considerable effort is being devoted to the development of the Liquid Metal Fast Breeder Reactor (LMFBR) as a future energy source. Although the LMFBR possesses some very attractive safety features -- like low coolant pressures and a normal coolant temperature far below the boiling point -- there is one characteristic that does raise concern: The core as constructed is not in its most reactive configuration. Relocation of nuclear fuel or sodium coolant can cause reactivity increases and severe power excursions if engineered safety systems should fail simultaneously. Therefore much attention has been given in LMFBR safety research to detailed mechanistic calculations of such Hypothetical Core Disruptive Accidents (HCDAs). The result of main interest is the mechanical energy release -- often termed excursion yield -- which is defined as the mechanical work done on the pressure vessel.

HCCA scenarios are generally subdivided in several phases, two of which are particularly important because they can result in a major threat to pressure vessel and containment integrity: energetic core disassembly and the subsequent core-expansion phase.

An energetic core disassembly occurs whenever the accident enters by some preceding events into a superprompt critical excursion [1]. In a few 10 milliseconds, temperatures around 5000 K and pressures of the order of 10 MPa can be reached,

causing an outward acceleration of the mostly liquid core materials. After the core volume increased by 5 to 10%, neutronic excursion and fission energy release are generally terminated.

In the now following core expansion phase the liquid-vapor mixture of core components continues to expand against the constraints of surrounding sodium and cold core structures. The expansion phase is terminated when the accelerated sodium slug impacts the vessel head, typically after several 100 ms.

It is a general belief that the reactor fuel - a uranium-plutonium mixed oxide - is the main working fluid in both described accident phases, because the fission energy is released in the fuel and only little time is available for heat transfer to sodium or stainless steel. So in order to couple the neutronic energy input into the fuel with hydrodynamic motions and temperature increases in the core, the U-p-v-T data of the fuel are needed.

2. DEFINITION OF RESEARCH GOAL

Although the complete U-p-v-T equation of state (EOS) of the nuclear fuel is required in principle for HCDA calculations, different parts of the fuel EOS have different degrees of importance. In this section the most important pressure information and the necessary precision will be identified. The $p(U,v)$ and $p(T,v)$ format is chosen here for representation of the fuel EOS.

2.1 Pressure Information Required in HCDA Calculations

In disassembly calculations two types of mesh cell situations are encountered:

1. The mesh cell is completely filled with liquids, or
2. the mesh cell contains free volume which can be filled with vapor.

In the first case, the cell pressure is generally dominated by the most compressible fluid present, which is normally sodium. Any single phase pressure from heated and expanding fuel is relieved by compressing the sodium in the cell. Thus the pressure determining material data for liquid filled cells are the fuel expansion coefficient -- which determines the degree of sodium compression -- and the sodium compressibility. Single phase pressures of the fuel have virtually no influence on calculated excursion yields [2].

In the case of a mixed phase mesh cell, the actual fuel vapor pressure can be saturated or undersaturated, depending on the vaporization kinetics. Refling, et al. [3] showed that

the net evaporation rate encountered during the core expansion phase is almost always one to two orders of magnitude smaller than the maximum possible rate. It is therefore adequate to assume thermodynamic equilibrium between liquid fuel and fuel vapor, that is saturation vapor pressures in the free volume of a mesh cell. Since net evaporation rates during the preceding disassembly phase are smaller than those of the core expansion phase, this conclusion is valid for the whole core disruptive accident.

2.2 Required Precision for Saturation Vapor Pressures

Now that the fuel saturation lines $p_{\text{sat}}(T)$ and $p_{\text{sat}}(U)$ have been identified as the most important parts of the $p(T, v)$ and $p(U, v)$ surfaces, the next step is to estimate the precision with which the saturation pressure needs to be known for HCDA calculations. Such a precision estimate will serve as the goal against which the accomplishments of the various theoretical and experimental methods can be compared. Since, so far, only intuitive feelings about the required vapor pressure precision were expressed -- often a factor of two -- a quantitative estimate is attempted here.

As mentioned before, the quantity of main interest in core disassembly calculations is the excursion yield Y . Uncertainties in the calculated yield arise from the uncertainty in the vapor pressure as well as from other accident variables like reactivity ramp rate $\dot{\zeta}$, Doppler coefficient D , etc. The total yield uncertainty δY can be written as:

$$\delta Y = \frac{\partial Y}{\partial P_{\text{sat}}} \cdot \delta P_{\text{sat}} + \frac{\partial Y}{\partial \dot{\zeta}} \delta \dot{\zeta} + \frac{\partial Y}{\partial D} \cdot \delta D + \dots \text{terms from other variables} \quad (1)$$

Sensitivity studies show that the dominant term in Eq. (1) is that from the ramp rate uncertainty $\delta \dot{\zeta}$ [4,5]. Obviously, the term from vapor pressure uncertainties should be some fraction "a" of this dominant term:

$$\frac{\partial Y}{\partial P_{\text{sat}}} \cdot \delta P_{\text{sat}} = a \cdot \frac{\partial Y}{\partial \dot{\zeta}} \cdot \delta \dot{\zeta} \quad (2)$$

A value of $a=.5$ appears as a reasonably balanced value. In sensitivity studies, the dependence of calculated excursion yields Y on the ramp rate $\dot{\zeta}$ was found to be

$$Y = c \cdot \dot{\zeta}^b \quad \text{where } b = 1.5 \dots 2.0 \text{ [4]} \quad (3)$$

Eq. (3) is based on excursion yields which were derived from an isentropic expansion of the superheated core bubble to a fixed cover gas volume (26 m^3). Such yield calculations, however, ignore energy loss mechanism during the bubble expansion, like e.g. heat transfer to sodium or constraints from the upper core structure. Inclusion of these effects will certainly tend to decrease the sensitivity of the excursion yield on the ramp rate at prompt critical, making b smaller than calculated in [4]. Unfortunately, there are no SIMMER studies available from which a more realistic exponent b could be evaluated. So Ostensen's lower limit of $b=1.5$ is chosen here. Inserting $\partial Y / \partial \dot{\zeta}$ from Eq. (3) into Eq. (2) yields

$$\frac{\partial Y/Y}{\partial P_{\text{sat}}/P_{\text{sat}}} \cdot \frac{\delta P_{\text{sat}}}{P_{\text{sat}}} = a \cdot b \frac{\delta \zeta}{\zeta} \quad (3a)$$

The relative sensitivity of the yield on the saturation vapor pressure $(\partial Y/Y)/(\partial P_{\text{sat}}/P_{\text{sat}})$ was calculated from the existing sensitivity studies [2, 4, 5, 6, 7, 8, 9]; the results are plotted in Figure 1 as a function of the ramp rate.

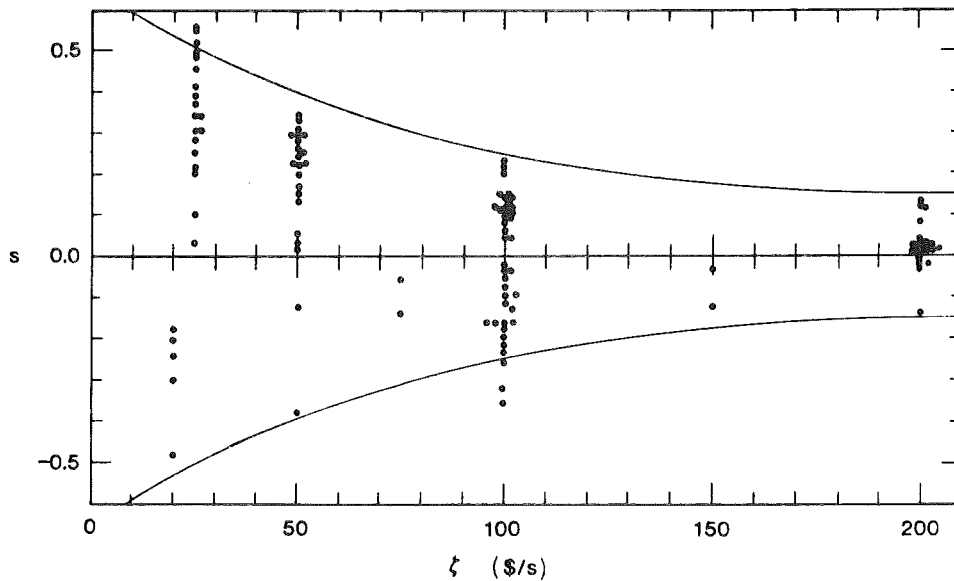


Figure 1. Relative sensitivity of calculated excursion yields on the fuel saturation vapor pressure [$s \equiv (\partial Y/Y)/(\partial P_{\text{sat}}/P_{\text{sat}})$] as function of ramp rate ζ .

The observed scatter reflects the influence of different p-T relations and additional disassembly parameters on the calculated excursion yields. As indicated by the two lines -- which bound the HCDA parameter space -- the yield sensitivity on the fuel vapor pressure generally decreases with increasing accident ramp rate. For any given accident, this sensitivity s is a constant and Eq. (3a) can be integrated with respect to

some reference case ($P_{\text{sat},0}$, $\dot{\zeta}_0$) to give

$$\frac{P_{\text{sat}}}{P_{\text{sat},0}} = \left(\frac{\dot{\zeta}}{\dot{\zeta}_0} \right)^{ab/s} \quad (4)$$

Eq. (4) defines by what factor ($P_{\text{sat}}/P_{\text{sat},0}$) the saturation vapor pressure may vary if the ramp rate of the accident is uncertain by the factor $\dot{\zeta}/\dot{\zeta}_0$. The final step is therefore to specify the ramp rate uncertainty $\dot{\zeta}/\dot{\zeta}_0$ which presently exists in typical calculations. In view of the large variety of different scenarios, it is not surprising that ramp rates are known better in some cases than in others. A distinction into two broad accident classes with different uncertainty ranges for $\dot{\zeta}$ seems therefore appropriate; namely:

1. $\dot{\zeta}/\dot{\zeta}_0 = .66$ to 1.5 (Level I precision) and
2. $\dot{\zeta}/\dot{\zeta}_0 = .83$ to 1.2 (Level II precision).

Using these ramp rate ranges together with $a=.5$, $b=1.5$ and the bounding lines for s from Figure 1 in Eq. (4) yields the pressure ranges shown in Figure 1a.

The result is that -- e.g., at a ramp rate of $50\$/s$ -- the two above specified ramp rate uncertainty ranges allow for a pressure uncertainty factor of 4 (Level I) and 2 (Level II), respectively. These pressure uncertainties for a ramp rate at $50\$/s$ can be considered a reasonable general goal for vapor pressure determinations because

- accidents with ramp rates above $50\$/s$ have a rapidly decreasing probability, and

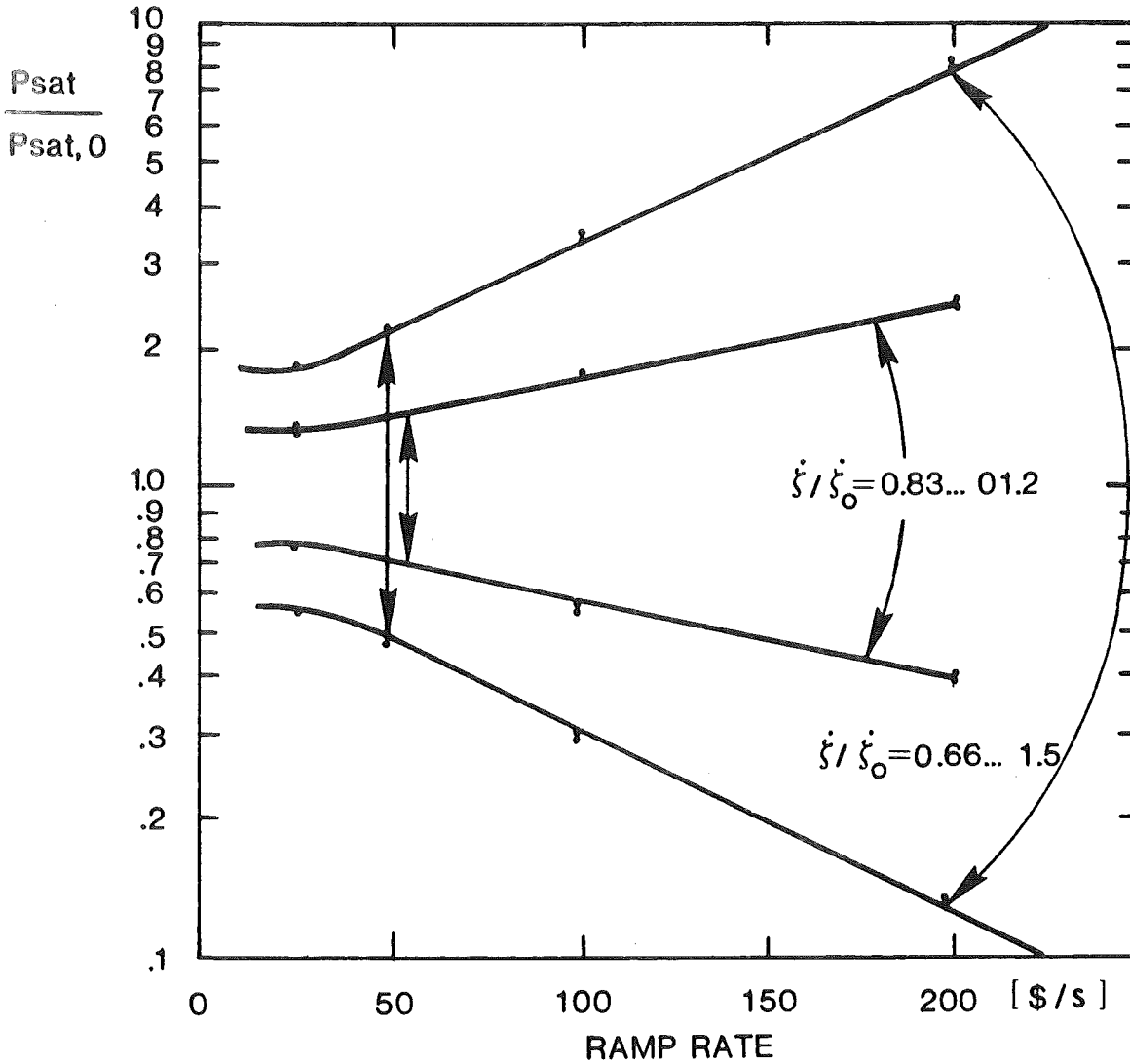


Figure 1a. Acceptable pressure uncertainty range $P_{sat}/P_{sat,0}$ for two fixed ramp rate uncertainties $\dot{\xi}/\dot{\xi}_0$ as function of the nominal accident ramp rate $\dot{\xi}_0$.

- accidents with ramp rates below 50 $[\$/s]$ are very likely to be confined within the pressure.

So in summary, the fuel saturation vapor pressure should be known within a factor of 2 if the ramp rate of the considered accident is known within the above defined Level-II precision. If the ramp rate is only known with the Level-I precision, a factor of 4 in the vapor pressure appears sufficient.

Due to the exponential relationship between temperature and pressure ($p = A \exp(-\Delta H/RT)$), the acceptable pressure

uncertainty translates into a very small acceptable temperature uncertainty, which is given by:

$$\frac{\delta T}{T} = \frac{RT}{\Delta H} \cdot \ln p/p_0 \quad \left(\frac{RT}{\Delta H} \approx .07 \right) \quad (5)$$

Meaningful vapor pressure measurements therefore require very precise temperature determinations. The acceptable uncertainty in the internal energy $\delta U/U$ follows from Eq. (5) by transforming temperature T into internal energy U . The results are summarized in Table I.

TABLE I

Precision Level	Uncertainty range in ξ/ξ_0	Acceptable pressure uncertainty p/p_0	or Acceptable temperature uncertainty $\delta T/T$ (at 4000 K)	or Acceptable internal energy uncertainty $\delta U/U$ (at 2000 J/g)
I	.66 to 1.5	4.0	$\pm .05$	$\pm .057$
II	.83 to 1.2	2.0	$\pm .025$	$\pm .029$

In the following sections, the achievements of the various methods for determining the fuel saturation vapor pressure will be compared to the goals listed in Table I.

3. REVIEW OF THEORETICAL METHODS

In this chapter the various theoretical methods used to determine liquid fuel vapor pressures will be reviewed. Theoretical basis, applications and a critical evaluation of each method will be given. Finally, the theoretical results obtained so far for UO_2 , will be assessed.

3.1 Corresponding States Theory

3.1.1 Outline of Theory

For a given class of particles -- e.g., rare gases or polar molecules -- a CST can be derived from statistical mechanics under a set of well-defined assumptions concerning molecular properties of the particle class under consideration. One assumption defines e.g., a form for the pair potential which is assumed to be common to all members of the class.

Using the given set of assumptions the configurational integral is rearranged to a form which depends only on dimensionless quantities. One can then define dimensionless thermodynamic properties (e.g., pressure p^*) and show that they are universal functions of dimensionless temperature T^* , volume v^* etc.

In the case of rare gases e.g., one defines a pair potential of the form

$$\phi(r) = \epsilon \cdot \psi\left(\frac{r}{\sigma}\right) \quad (6)$$

where constants ϵ and σ are characteristic for a given rare gas while the shape function ψ is assumed to be common to all rare gases. One then finds the relation

$$p^* = g(T^*, v^*) \quad (7)$$

where the dimensionless variables turn out to be

$$p^* = p\sigma^3/\epsilon, \quad T^* = kT/\epsilon \quad \text{and} \quad v^* = v/\sigma^3 \quad (8)$$

and g is a universal function for all rare gases.

It can be shown that the molecular reducing parameters in Eqs. (8) are not the only possible ones, also the critical constants p_c , T_c and v_c are a set of valid scaling parameters. With $p_r = p/p_c$ etc., Eq. (7) can be rewritten as

$$p_r = f(T_r, v_r) \quad (9)$$

If the function f is known from p - v - T data and reducing parameters of one class member, the p - v - T behavior of other members -- which have not been studied experimentally -- can be predicted, provided their reducing parameters are known. The Simple CST of Eqs. (7) or (9) is very well obeyed by Ar, Kr and Xe, indicating that Eq. (6) is entirely adequate for describing the pair potential of these monatomic fluids. Simple CST applies moderately well for N_2 and CH_4 , but fails for other polyatomic molecules, even symmetric ones like CF_4 or CCl_4 [10]. Improvements beyond Simple CST are therefore desirable. However, the derivation of a corresponding states formalism becomes very difficult with refined assumptions on the molecular behavior e.g., a more appropriate pair potential in Eq. (6). This led to empirical refinements of Simple CST, where Eq. (9) is formally extended to the form

$$p_r = f(T_r, v_r, X) \quad (10)$$

The third dimensionless variable X is supposed to account for all deviations of polyatomic properties from Eq. (9). Several choices have been proposed for X . Hougen et al. [11] selected the compressibility factor at the critical point

$$X \equiv Z_c = \frac{p_c v_c}{RT_c}, \quad (11)$$

because Z_c has a single value for all molecules obeying the Simple CST. They also presented tables for the function f in Eq. (10). So in order to derive unknown p - v - T data of a given substance, first its critical data need to be estimated. Equation (11) then defines the empirical class to which the substance should belong and Eq. (10) describes the reduced behavior of this class.

3.1.2 Applications

Several authors have applied the Generalized CST of Eqs. (10) and (11) to UO_2 [12, 13, 14, 15, 16]. As shown above, the problem of deriving UO_2 vapor pressures from CST reduces to estimating the critical constants of UO_2 . A number of empirical relations are used for this purpose, e.g., the law of rectilinear diameters or the Riedel equation (see e.g. Reference 16), relations which are largely based on the properties of organic or simple covalent inorganic liquids. Figure 2 summarizes the calculated results for $p_{sat}(T)$, and Figure 11 those for $p_{sat}(U)$.

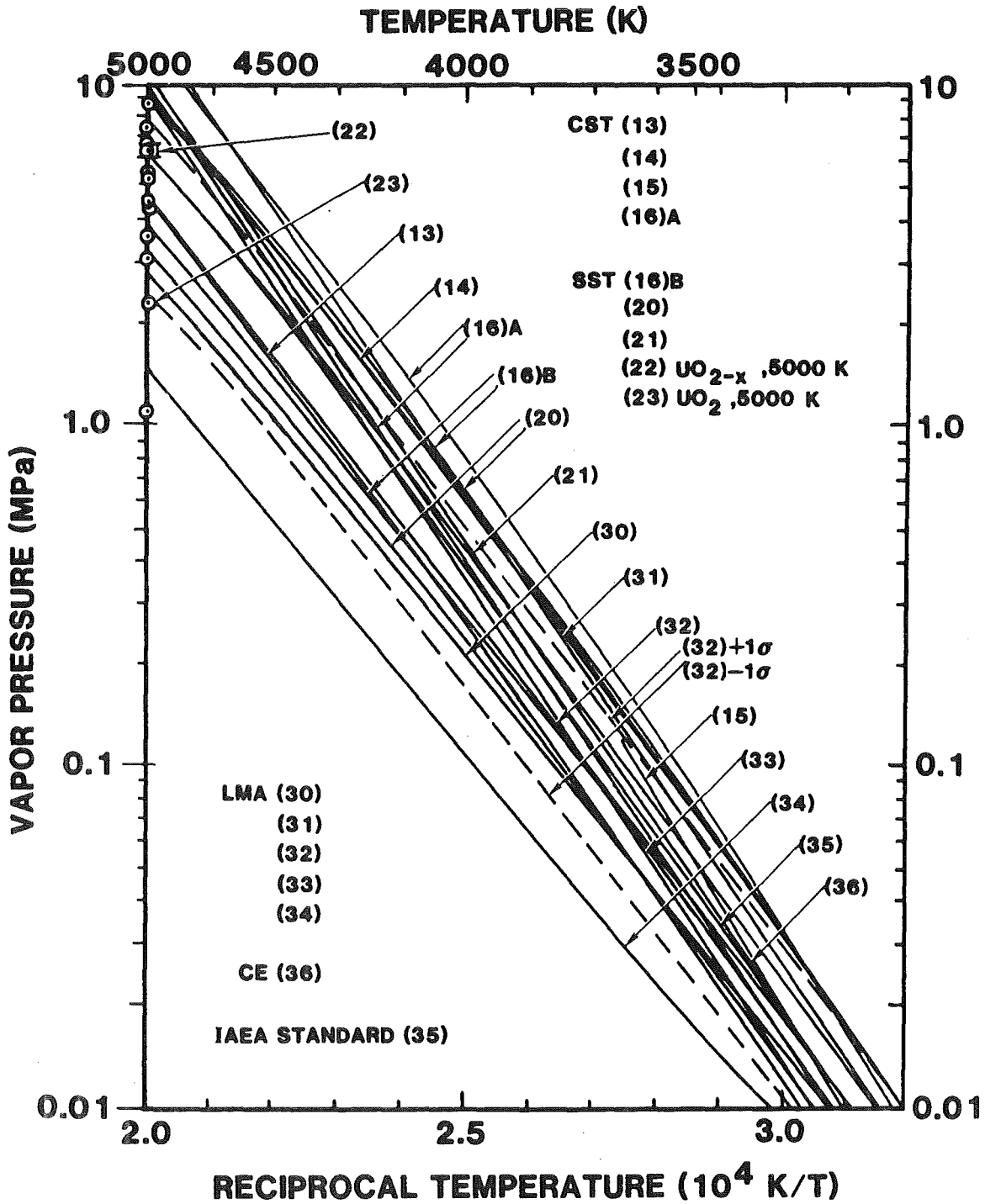


Figure 2. Calculated saturation vapor pressures of liquid UO_2 as function of reciprocal temperature.

3.1.3 Evaluation of Method

While Simple CST (Eq. 7) has a sound theoretical basis, Generalized CST (Eqs. 10 and 11) is empirical in nature. For instance, the only two metals for which the critical data are established -- namely mercury and cesium -- possess vastly different critical compressibilities and therefore do not belong to the same CST class [17]. It is only by experience that some confidence for Generalized CST could be obtained for certain classes of fluids, e.g., hydrocarbons in the chemical industry. When Generalized CST is applied to a member of a class of fluids which is not represented in the empirical data base -- like liquid oxides -- the results may or may not be close to the actual properties. Decisive is the degree of molecular similarity between the reference liquids (largely organic) and the liquid under consideration (UO_2). Unfortunately, this similarity seems to be poor in the case of liquid UO_2 .

Three major differences are listed here:

- Solid UO_2 is generally believed to be highly ionic, thus pair potentials in liquid UO_2 are likely to differ substantially from those of the organic reference liquids.
- At temperatures above 3700 K thermal ionization of UO_2 vapor becomes noticeable, leading to changes in the effective intermolecular potential of the vapor [18].
- UO_2 vaporization is not a single component phase transition but accompanied by chemical reactions, which lead

to a multicomponent gas phase with an overall composition which is different from that of the liquid. These characteristics of the UO_2 system are not represented in the empirical data base of Generalized CST.

Besides this fundamental problem a severe practical one exists also: there is at present no means of estimating the critical constants of UO_2 with the necessary precision. The scatter existing in the different CST results (Figures 2 and 11) is mainly a consequence of the different critical data used in scaling the Generalized EOS in Eq. (10). So mere application of the General CST data base to UO_2 is afflicted with significant uncertainties in the results.

3.2 Significant Structures Theory

The Significant Structures Theory (SST) of liquids as developed by Eyring [19] provides another method for the estimation of liquid fuel vapor pressures.

3.2.1 Outline of Theory

A liquid is pictured as being a mixture of "solid-like" and "gas-like" molecules. A molecule has solid-like properties as long as it vibrates about an equilibrium position and gas-like degrees of freedom when it jumps into a neighboring vacancy. With this model in mind the total partition function of the liquid Z_ℓ is written as

$$Z_\ell(V, T) = Z_s^{NV_s/V} \cdot Z_g^{N(V-V_s)/V} \quad (12)$$

The gas partition function Z_g is constructed in the usual way as product of translational, vibrational, rotational and electronic factors. The solid partition function Z_s is modified in two ways, as a result of the underlying SST model:

- a solid-like molecule in the liquid has no longer only one single equilibrium position, but a number of additional quasi-equilibrium positions, and
- to account for long range forces -- as present in ionic liquids -- the binding energy in Z_s is made to depend on the mean liquid density.

The Helmholtz free energy A is found from Z_ℓ according to the standard relation:

$$A(V,T) = -kT \ln Z_\ell (V,T) \quad (13)$$

Using the definition $p = - (\partial A / \partial V)_T$, the equilibrium vapor pressure between liquid and gas phase at a given temperature T is then obtained from a $A(V)_T$ plot as the slope of the common tangent between the points $A(V_\ell)$ and $A(V_g)$.

3.2.2 Applications

Several authors applied Significant Structure Theory to liquid UO_2 [16,20,21,22,23]. In order to assess the validity of SST for an ionic substance such as UO_2 , Gillan [20] predicted vapor pressures for eight liquid alkali halides for which experimental data are available. With known vapor pressures over the solid serving as input data, the calculated vapor pressures over the liquid agreed with the measurements within

a factor of 2. This is comparable to the experimental resolution and thus totally satisfactory. Since the original SST assumes congruent evaporation [i.e., $\text{UO}_2(\lambda) \rightarrow \text{UO}_2(\text{g})$], Fischer [22] extended the SST approach to substoichiometric UO_{2-x} , allowing for $\text{UO}(\text{g})$ and $\text{UO}_2(\text{g})$ in the vapor phase. The SST results for $p_{\text{sat}}(\text{T})$ and $p_{\text{sat}}(\text{U})$ are summarized in Figures 2 and 11.

3.2.3 Evaluation of Method

For the construction of the solid-like partition function, measured vapor pressures over solid UO_2 and thermodynamic data of the melt-transition are used. Unfortunately the present precision in these data is unsatisfactory from a SST standpoint, and selections must be made.

For construction of the gas-like partition function molecular data for the UO_2 molecule are needed. The principal uncertainties in the gas partition function result from vibrational and electronic contributions. Two difficulties exist with the vibrational partition function [24,25]. The first is determination of reliable vibration frequencies -- especially that of the bending mode -- which can give rise to large uncertainties in the total vibrational contribution. The second problem concerns the importance and mathematical treatment of anharmonic vibration terms.

The electronic partition function is also difficult to calculate, mainly because in heavy metal oxides like UO_2 :

- a large number of low lying electronic states exist,
- many electronic states are occupied at the high tempera-

tures of interest, and

- no sufficiently accurate model for the electronic structure can be developed from the small amount of available data [25].

Because the electronic contributions to the total gas partition function are quite large, electronic uncertainties become important for the calculated SST results.

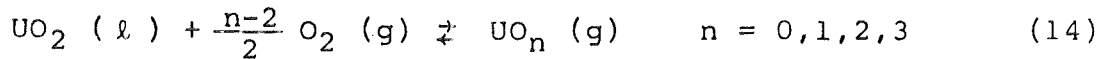
In a recent sensitivity study [23] the electron densities for the gaseous UO_2 molecule were varied within reasonable limits, while the solid-like partition function was kept fixed, using the latest recommendations for the solid properties [26]. The resulting vapor pressures at 5000 K vary by a factor of 8 as indicated in Figure 2. Also the large influence of the solid-like partition function is demonstrated by these calculations. The lowest point (1.1 MPa at 5000 K) and the curve from Reference 21 (6.3 MPa at 5000 K) were obtained with different values for ΔH_{sub} and p_{sat} , but very similar electron densities.

Besides the high sensitivity to the input data, a more fundamental problem with the application of SST to UO_2 is, that the underlying model for the liquid (Eq. 12), as well as the semi-empirical expression used for the solid-like partition function, lack experimental confirmation. The good results found for liquid alkali halides [20] lend some support to the SST approach, provided that high temperature or high pressure phenomena present in the UO_2 case, do not interfere with the basic SST assumptions.

3.3. Law of Mass Action

3.3.1 Outline of Theory

The equilibrium vapor pressure of gaseous species evaporating from a condensed phase can be calculated from the evaporation reaction. For the evaporation of U, UO, UO₂ and UO₃ molecules from liquid UO₂ the reaction reads:



The Law-of-Mass-Action (LMA) relates equilibrium activities of reactants and products with the free enthalpy change in Eq. (14). If the gas activities are taken as the gas pressures, the following relation is found for the pressure of gaseous UO_n:

$$p_{\text{UO}_n} (T) = \exp \left[\frac{\Delta G_f^\circ [\text{UO}_2(\ell)] + \frac{n-2}{2} \Delta \bar{G}_{\text{O}_2} - \Delta G_f^\circ [\text{UO}_n(\text{g})]}{RT} \right] \quad (15)$$

The numerator in Eq. (15) is simply the change in free enthalpy associated with the transfer of liquid UO₂ and gaseous oxygen into gaseous UO_n (n = 0, ..., 3). If the free enthalpy functions are known, the partial pressure p_{UO_n}(T) can be calculated.

The oxygen partial pressures in the vapor phase follow from the analogous LMA expressions:

$$p_{\text{O}_2} = \exp \left(\Delta \bar{G}_{\text{O}_2} / RT \right) \text{ and} \quad (16)$$

$$p_{\text{O}} = \exp \left[(1/2 \Delta \bar{G}_{\text{O}_2} - \Delta G_f^\circ (\text{O})) / RT \right] \quad (17)$$

The total saturation vapor pressure is then the sum of all partial pressures following from Eqs. (15) to (17):

$$P_{\text{sat}} = P_U + P_{\text{UO}} + P_{\text{UO}_2} + P_{\text{UO}_3} + P_{\text{O}_2} + P_{\text{O}} \quad (18)$$

3.3.2 Applications

Rand and Markin [27] were the first to apply the LMA method to solid (U, Pu) O_{2-x}. Later, workers at ANL applied this approach to UO₂, using thermodynamic functions for the gaseous species UO_n, which they derived from matrix isolation studies [28,29,30]. When new thermodynamic data for solid UO₂ and gaseous UO_n were recommended in 1974, the LMA method was tested against all available vapor pressure data of solid oxide fuels and since very encouraging agreement was found, the calculations were extended up to 5000 K [31].

It is obvious from Figure 2 that the various LMA results for liquid UO₂ are quite different. This due to the fact that each of the required thermodynamic functions is subject to uncertainties -- partly due to scatter in published data, partly due to necessary extrapolations of unknown data using theoretical models, e.g., for $\Delta\bar{G}_{\text{O}_2}$. The next step in LMA application was therefore a more statistical approach, which tried to identify the most probable region for $p_{\text{sat}}(T)$ in the following way [32]:

- all available data for a given thermodynamic quantity x_i , say $\Delta G_f^\circ [\text{UO}_2(l)]$, were plotted on one graph as function of temperature,

- from this plot a most probable value \bar{x}_i (T) and an associated standard deviation $\sigma_{x_i}(T)$ were chosen, and
- assuming a Gaussian distribution of x_i around the most probable value \bar{x}_i , the standard deviation of the total vapor pressure p_{sat} was calculated from the familiar variance propagation relation

$$\sigma_{P_{\text{sat}}}^2 = \sum_i \left(\frac{\partial P_{\text{sat}}}{\partial x_i} \right)^2 \cdot \sigma_{x_i}^2 \quad (19)$$

Figure 2 shows the resulting most probable vapor pressure curve for UO_2 together with the $1-\sigma$ confidence interval calculated from Eq. 19. The total vapor pressure of UO_2 can be expected to lie within this band with a probability of about 70%.

Recent work at ANL led to a new equation for ΔG_f° of liquid UO_2 [33] (which turned out to be very close to the "most probable" one chosen in [32]). When used together with other existing data in LMA calculations, the vapor pressure curve shown in Figure 2 was obtained.

The latest LMA-type calculation was performed by Long et al. [34]. Special emphasis was devoted on deriving a consistent set of heat capacity data for solid, liquid and gaseous UO_2 , which was then used to calculate the respective free energy functions. The total vapor pressure over UO_2 turned out to be quite low (Figure 2).

3.3.3 Evaluation of Method

The LMA method is a transparent approach which is based on a proven physical law.

It contains no empirical parameters and is the only theoretical method that fully includes the chemical reactions which are associated with the equilibrium evaporation of nuclear oxide fuels. It also allows in principle -- contrary to CST and SST -- a quantitative estimate of the uncertainties involved. However at present, the data basis for temperatures above 3000 K is such that, most probable value and standard deviations of the required quantities depend somewhat on personal judgement. They could change as new thermodynamic data become available.

It was agreed [35] that the LMA method should be applicable up to about 80% of the critical temperature (~4800-7200 K). Beyond this limit it may no longer be permissible to replace the gas activities in the Law-of-Mass-Action by the gas pressure, as done in deriving Eq. (15). However, this temperature range up to around 5000 K is sufficient; temperatures closer to the critical region -- where the LMA approach breaks down -- are not of interest for HCDA calculations.

3.4 Clapeyron - Equation

3.4.1 Outline of Theory

The Clapeyron - Equation

$$\frac{dp}{dT} = \frac{(H_v - H_c)p}{RT^2} \quad (20)$$

describes the variation of the saturation vapor pressure with temperature for a one-component liquid-vapor equilibrium.

In using Eq. (20) for UO_2 , it is implicitly assumed that the vapor phase consists of UO_2 molecules only. If H_c and H_v , the enthalpies of condensed and gaseous UO_2 , are known, Eq. 20 can be integrated to give $p_{\text{UO}_2}(T)$.

3.4.2 Applications

Workers at Los Alamos [36,37] used measured enthalpy data (up to 3600 K) and a linear extrapolation for higher temperatures to evaluate H_c .

The enthalpy function of the gas phase was constructed from theoretical models. The vibrational enthalpy contribution was based on measured vibration frequencies of UO_2 [24]. In evaluating the electronic partition function, a new density of electronic states was postulated, which lead to a very significant electronic contribution to H_v above 3000 K. Using the so derived H_v and fitting two constants in H_c to vapor pressure data of solid and liquid UO_2 , the authors were able to reproduce laser measurements on liquid UO_2 , described later [51].

3.4.3 Evaluation of Method

The previously discussed LMA method gives for the temperature dependence of the saturation vapor pressure

$$\frac{dp_{\text{sat}}}{dT} = \frac{dp_{\text{UO}_2}}{dT} + \frac{dp_{\text{UO}_3}}{dT} + \frac{dp_{\text{O}}}{dT} + \dots \quad (21)$$

It can now be shown that the Clapeyron-Equation a differential

form of Eq. (15) with $n = 2$. Therefore, Eq. (20) just represents the first term on the right side of Eq. (21), neglecting the contributions to dp_{sat}/dT from other vapor species. The most important ones are those of gaseous UO_3 and atomic O. In order to quantify the consequences of this neglect, the magnitudes of the three terms in Eq. (21) were evaluated from available LMA calculations [30,31]. Depending somewhat on temperature and thermodynamic input data, UO_3 and O together contribute generally 50 to 100% of the UO_2 term to dp_{sat}/dT . Therefore, Eq. (20) should significantly underpredict the slope of the saturation vapor pressure curve, and even more the integrated $p_{\text{sat}}(T)$. (This was indeed found in an earlier attempt using Eq. (20) for the calculation of $p_{\text{sat}}(T)$ [21] and the authors rejected the result). The here described Clapeyron-Equation approach is able to reproduce measured vapor pressures only, because the neglect of additional terms in Eq. (21) is compensated by a large value for dp_{UO_2}/dT , which is due to a new postulated electronic density of gaseous UO_2 . This electronic density has not been verified experimentally.

In summary the Clapeyron-Equation method is a simplified LMA approach which neglects important vapor species. The method is not capable of yielding results beyond those of complete Law-of-Mass-Action calculations.

3.5 Assessment of Theoretical $p(T)$ Results

Figure 2 summarizes the theoretical results for the saturation vapor pressure of UO_2 . In the first instance, the existing degree of coincidence is surprising, considering the

very different natures of the various theoretical approaches. However it must be remembered that available data on the vapor pressure of solid UO_2 ($p(T), \Delta H_{\text{sub}}$) and on the melt transition (ΔH_{fus}) predetermine a certain vapor pressure region for liquid UO_2 .

At 5000 K, the UO_2 vapor pressure can be expected somewhere between 1.5 and 15 MPa. All curves of Figure 2 fall into this predetermined pressure interval. It can therefore be concluded that the scatter in Figure 2 does not represent the full scatter in theoretical results, rather it is the scatter in those results which were felt to be compatible with already existing vapor pressure information.

The true value of a theory depends on its ability of further narrowing down the factor-of-10 band towards the goals defined in section 2. The following assessment of the various theoretical methods gives special attention to this ability.

3.5.1 Corresponding States Theory

The published saturation vapor pressures from CST differ by a factor of 3. These differences mainly originate from the different sets of critical UO_2 data, used in Generalized CST (Eqs. 7 and 8).

At present no experimental or theoretical basis exists for favoring one particular set of critical data over any other proposed set.

An additional more fundamental source of uncertainty lies in the empirical nature of Generalized CST. As discussed in

section 3.1, there probably exists little molecular similarity between the reference liquids and liquid UO_2 , so that the empirical CST data basis for predicting UO_2 properties may not be applicable. The errors associated with applying the CST data to liquid UO_2 are not amenable to a quantitative estimate. So aside from the above mentioned factor of 3, an additional uncertainty of unknown size exists. It is not safe to say that the true UO_2 vapor pressure is within a factor of 4 around any CST pressure curve; thus, in the author's opinion, General CST results do not meet the Level I precision (factor of 4 in pressure).

3.5.2 Significant Structure Theory

SST results for UO_2 vapor pressure depend strongly on the particular set of input data. In Fischer's work [21,23] the calculated vapor pressure changed by a factor of 6 at 5000 K when the solid input data were adjusted to the most recent recommendations. A not unreasonable variation in the electron densities caused vapor pressure differences of a factor of 8 at 5000 K.

Furthermore, it must be remembered that SST is a semi-empirical approach for picturing the behavior of a liquid. Although the basic assumption (Eq. 12) and the intuitively modified partition function of the solid-like molecules allowed a successful description of properties for quite a number of substances, SST is by no means a universally proven approach. Systematic errors cannot be excluded when SST is applied to

an exotic liquid like UO_2 , aside from the above mentioned input data uncertainties. In the author's opinion, the SST vapor pressures published so far, do not allow to locate the true UO_2 vapor pressure within a factor of 4.

3.5.3 Law of Mass Action

The LMA method is based on a proven physical law, contains no free parameters and fully describes the chemical reactions associated with equilibrium vaporization of UO_2 . If the uncertainties in the input data are known, the uncertainty in the calculated saturation vapor pressure can be estimated also. The first attempt in narrowing down the probable vapor pressure region gave a factor of 3 for the 1- σ band [32]. Since the 1- σ band corresponds to only 70% confidence, there is still a 1:3 chance to find the actual vapor pressure outside this band. The 2- σ band, which corresponds to 95% confidence, extends in these calculations from essentially 0 to 10 MPa at 5000 K, a not very conclusive result. So the standard deviations of the input data need further reductions before the 2- σ band -- which would be a really conclusive band -- can meet the requirements defined in section 2.

3.5.4 Clapeyron-Equation

The CE approach is a simplified LMA method which only considers gaseous UO_2 and which makes an unacceptable neglect of important vapor species like UO_3 and O.

The results obtained in [36,37] merely demonstrate that measured vapor pressure data can be fitted by postulating

a very high electronic contribution to the enthalpy of gaseous UO_2 . The CE calculations did not yield new independent results for the partial pressure of gaseous UO_2 and clearly not for the complete saturation vapor pressure of liquid UO_2 which is of interest for the HCDA analysis.

3.5.5 Summary

Despite substantial theoretical efforts, none of the above discussed methods is presently capable of locating the factor-of-4 vapor pressure band (Level I precision) which contains the true UO_2 vapor pressure without doubt. In this situation it appears reasonable to recommend the IAEA standard [35] because this line is close to the average of all published results.

Of the different theoretical methods, the Law-of-Mass-Action seems to offer the most direct way to achieving this goal because uncertainties in LMA results come from input data uncertainties only. Results obtained with Generalized CST or SST underly additional unresolved uncertainties, based on the theoretical models themselves. Further research needs for the theoretical methods will be discussed in section 6.1.

4. REVIEW OF EXPERIMENTAL METHODS

Up to 1972, vapor pressure data of liquid oxide fuels were purely based on the theoretical models described above. Since then, groups at several laboratories developed new techniques for measuring vapor pressures in the liquid range. These techniques and the results obtained will be reviewed in the following sections.

4.1 ANL* Transpiration Technique

Measuring Principle

A weighted amount of UO_2 is heated to a desired temperature and an inert gas is passed over the sample (Figure 3). This gas carries the vapor species into a cold tube where the uranium bearing molecules condense. After the experiment the total amount of uranium oxide collected in the tube is determined by wet chemistry.

Quantities measured in this method are the number of uranium moles transported, n_u ; number of moles of carrier gas passed through the system, n_c ; and total system pressure, P_T .

Data Evaluation

The total pressure of uranium bearing species, P_u , is calculated from the additivity of partial pressures:

$$P_T = P_C + P_u = P_u \left(1 + \frac{P_C}{P_u} \right) = P_u \left(1 + \frac{n_C}{n_u} \right) \quad (22)$$

Figure 4 shows the results for liquid uranium oxide [38]. Each

*Argonne National Laboratory, Illinois, USA

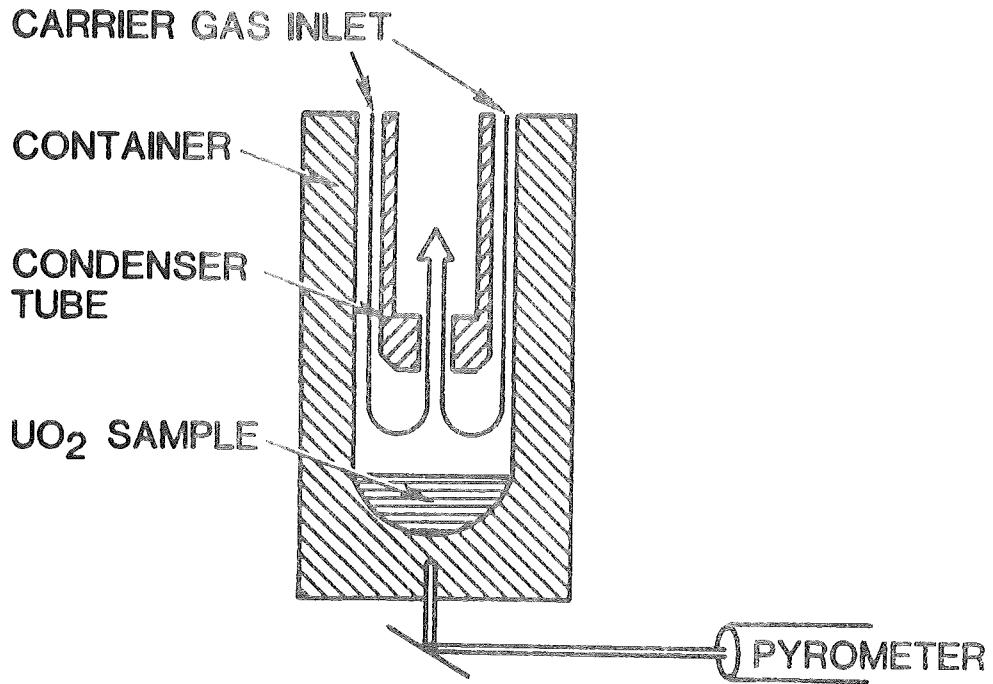


Figure 3. ANL Transpiration Technique

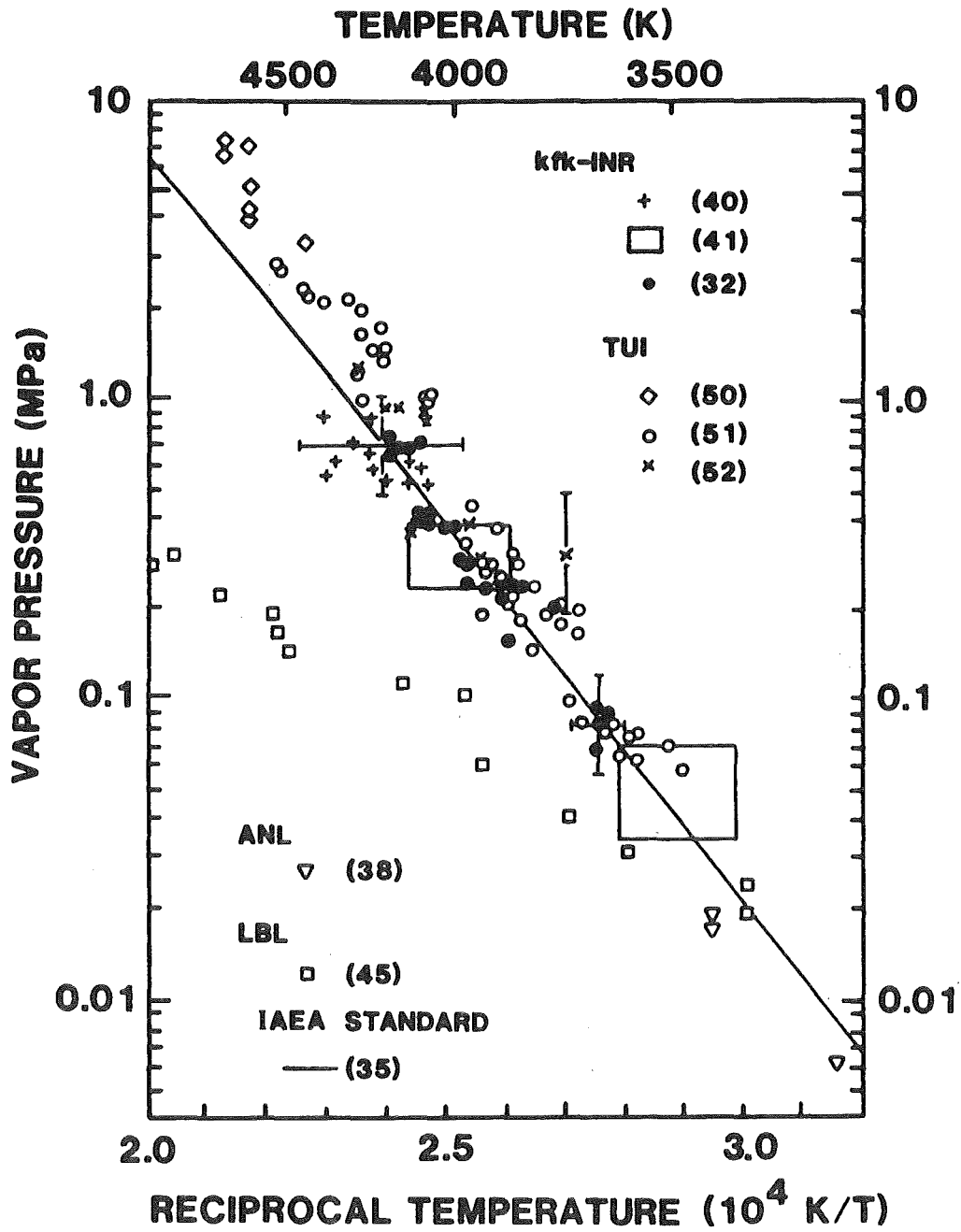


Figure 4. Measured vapor pressures of liquid UO_2 as function of reciprocal temperature.

point is a mean value from several runs, the average deviation from the mean being about $\pm 10\%$. No temperature uncertainties are quoted.

Evaluation of Method

In order to obtain saturation vapor pressures from Eq. (22), the partial pressure of UO_n in the carrier gas must be equal to the saturation partial pressure, which exists at the liquid-gas interface.

Clearly the degree of saturation in the carrier gas depends on the gas flow rate. Too high flow rates result in under-saturation and apparent low vapor pressures; whereas, too low flow rates yield high vapor pressures due to self and/or thermal diffusion effects in the gas mixture [39]. In a properly designed transpiration apparatus, a range of flow rates exists where the measured vapor pressures are independent of the flow rate; in this range the saturation condition is considered to be met.

Carrier gas saturation appears to be given in the ANL experiments [38] because the results obtained for solid UO_2 agree with those of other techniques within the experimental uncertainties.

The data shown in Figure 4 are those of UO_{2-x} because the O/U ratio dropped from 2.00 to 1.94 during the transpiration runs. Law-of-Mass-Action calculations indicate a 15% pressure increase in going from O/U = 1.94 to 2.00 [31].

4.2 Laser Surface Heating

4.2.1 KfK-INR* Technique

Measuring Principle

The measuring principle is outlined in Figure 5. A 1 to 10 millisecond long pulse is chopped from a continuous CO₂ laser beam ($\lambda = 10.6 \mu\text{m}$) and focused through a transparent pendulum onto the surface of a fixed UO₂ target. A wobble mirror causes the laser beam to describe a circle on the UO₂ surface. The off-streaming vapor is collected by a ballistic pendulum which is suspended from a microbalance. The pendulum amplitude is recorded photographically. Thus total momentum as well as total mass of the vapor plume are measured in this technique.

A fast micropyrometer is used to determine the radial temperature distribution in the laser crater $T(r)$ and the course of the central crater temperature during the experiment.

Data Evaluation and Results

The quantities of interest are evaluated with a gas dynamic model which consists of the following steps [32,40,41]:

- From measured mass and momentum of the vapor plume an effective average vapor velocity W_{eff} follows immediately,
- W_{eff} is then converted to the final vapor molecule velocity, W , using the angular mass distribution in the vapor jet as given by Laval's theory for Mach-1 nozzles,

*Kernforschungszentrum Karlsruhe - Institute for Neutron Physics and Reactor Technology, FRG.

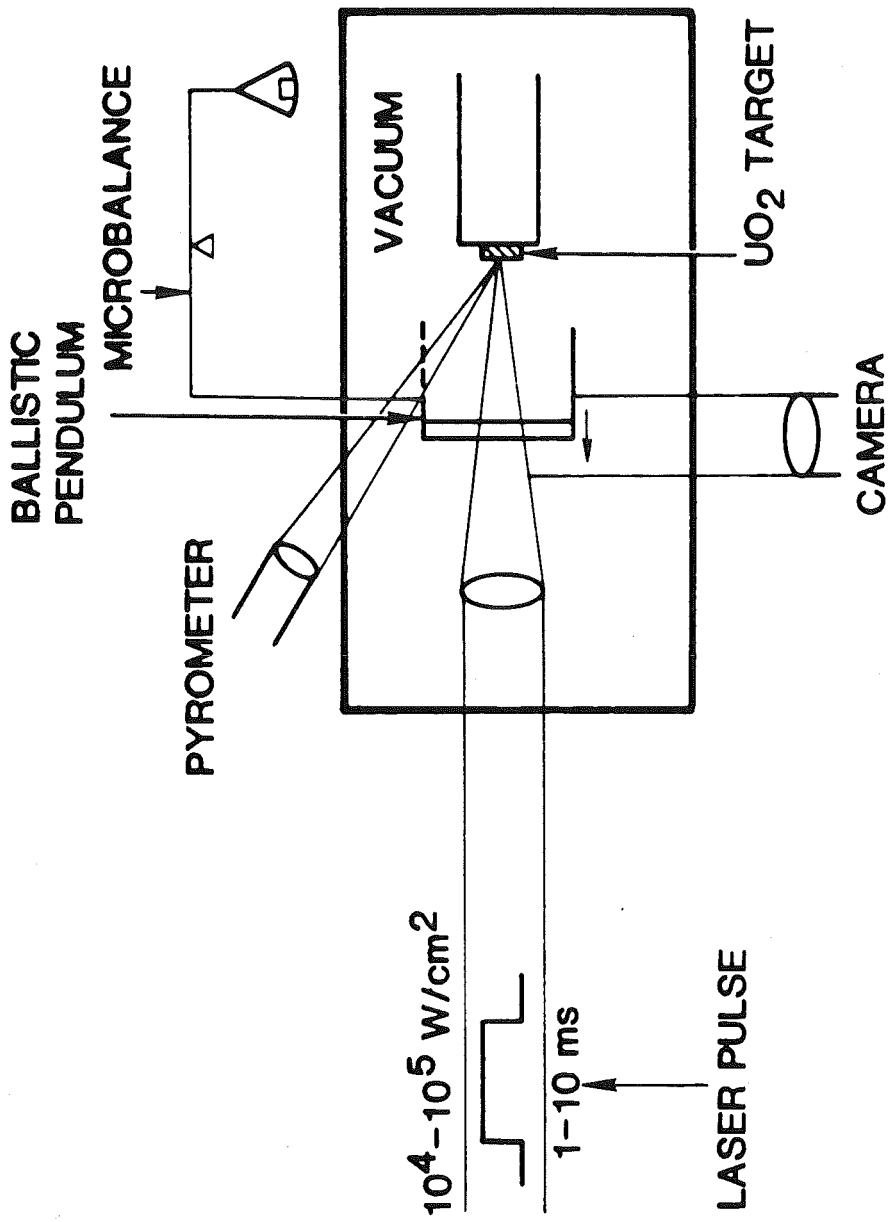


Figure 5. KfK-INR Laser Heating Technique (Vacuum Evaporation).

- Assuming that W_{eff} was obtained by adiabatic relaxation of translational and rotational degrees of freedom (=5 for UO_2) the initial temperature of the vapor molecules, T_v , in the layer directly above the surface is obtained,
- The vapor density in this layer, ρ_v , follows from mass conservation: the measured mass flux leaving the surface (\dot{m}/F) is equal to the mass flux in the vapor regime ($\rho_v \cdot W$),
- The vapor pressure in the boundary layer, p_0 , is then evaluated from ρ_v , T_v , and the ideal gas law,
- This p_0 is related to the required saturation vapor pressure by

$$P_{\text{sat}} = p_0 \cdot \frac{2}{1+b} / \frac{\alpha_c}{1-b(1-\alpha_c)} \quad (23)$$

which was deduced from established gas-dynamic relations. The condensation coefficient, α_c , is defined as "condensing particle flux/incident particle flux" and b is the probability for self-back scattering of vapor molecules. $\alpha_c = 1$ and $b = .4$ were used in the pressure evaluation.

In the later experiments [32], the gas dynamic vapor temperature determination (above first three steps) was replaced by the more accurate pyrometric temperature measurement. In addition, the radial temperature profile in the laser crater was accounted for by an iterative formulation of the last

three steps in the above described evaluation procedure.

Figure 4 shows the results obtained with the KfK-INR technique. Uncertainties in the first set of data points around 4200 K [40] were estimated to $p/p_0 = .7$ to 1.5 and $T/T_0 = .94$ to 1.06, they are indicated in Figure 4 for one data point.

The value for p/p_0 was obtained from Eq. (23) with $.7 \leq \alpha_c \leq 1$ and $.25 \leq b \leq 1$. The temperature uncertainty corresponds to an uncertainty in the relaxing degrees of freedom of about $\pm 1/2$. Later measurements on the vapor jet structure [48] confirmed the range of relaxing degrees of freedom used in the above gas dynamic temperature determination, namely $f_{\text{relax}} = 5 \pm 1/2$.

Subsequent experiments at lower temperatures yielded data points within the two indicated rectangles [41]. Uncertainties for these results are the same as given above. The third series of experiments [32] used optical pyrometry instead of gas dynamic temperature determination. The required UO_2 emissivity for the pyrometer wavelength (.63 μm) has been measured by the same group up to 4200 K with an integrating sphere technique, using the same pyrometer and temperature calibration procedure as in the laser evaporation experiments [42,43]. The temperature uncertainty is estimated to $\pm 1.5\%$ and the pressure uncertainty again to $p/p_0 = .7$ to 1.5. These uncertainty bounds are shown in Figure 4 for one point of the third measuring series.

Due to the laser induced changes in the surface composition of the sample, the measured pressures should be attributed

to substoichiometric uranium oxide (see section 4.3 for discussion).

Evaluation of Method

The following discussion is divided into pressure and temperature evaluation in the KfK-INR method.

The pressure evaluation is based on a gas dynamic model which addresses the essential phenomena encountered in the free supersonic flow of vapor into vacuum. The pressure uncertainties from the unknown model parameters α_c and b were estimated to about a factor of two ($p/p_0 = .7$ to 1.5 in Figure 4). The systematic uncertainties of the model from simplifying assumptions about the gas dynamic processes were estimated by the responsible author to another factor of 2 [44]. Adding these independent uncertainty contributions quadratically yields a pressure uncertainty of a factor of 2.8. Since there still is the possibility that α_c or b are outside the assumed ranges ($.7 \leq \alpha_c \leq 1$ and $.4 \leq b \leq 1$), it must be concluded that the overall pressure uncertainty in the KfK-INR technique is somewhat larger than a factor of 3.

The pyrometric temperature evaluation in laser experiments is based on the equation

$$E_\lambda = (1-a) \cdot \epsilon \cdot 2\pi c^2 h \lambda^{-5} / [\exp(ch/k\lambda T) - 1] \quad (24)$$

where

E_λ = spectral power density of the emitting surface as measured with pyrometer ($W/m^2 \mu m$)

a = fraction of light emanating from the laser crater
which is absorbed in the UO₂ vapor plume

ε = UO₂ emissivity at the pyrometer wave length

The last factor in Eq. (24) is Plank's Law. If E_λ, a and ε are known, T can be determined. Uncertainties in T originate from each of these three quantities. By differentiating Eq. (24) with respect to these variables, one finds that the temperature uncertainty ∂T/T resulting from an uncertainty in E_λ, a or ε, may be written as:

$$\frac{\partial T}{T} = \frac{T}{B} \cdot \frac{dE_{\lambda}}{E_{\lambda}}, \quad \frac{\partial T}{T} = \frac{T}{B} \cdot \frac{da}{1-a}, \quad \frac{\partial T}{T} = -\frac{T}{B} \cdot \frac{d\epsilon}{\epsilon} \quad (25a-c)$$

where B = ch/kλ = 22843 K. The differential form of Eq. (25) is sufficiently precise for the present discussion.

Uncertainties in measuring E_λ come from various sources, they were estimated to dE_λ/E_λ = ± 2% [44]. The absorption of optical radiation in the laser induced vapor plume was neglected in the temperature evaluation, i.e., a = 0 was assumed. This point will be discussed in more detail in section 4.3.

The emissivity of liquid UO₂ has been measured up to 4200 K with an estimated uncertainty of ± 1.5% [43]. If one adds the random errors from E_λ and ε quadratically, Eq. (25) gives a temperature uncertainty dT/T of about ± .5% between 4000 and 5000 K. This extremely high precision of pyrometric temperature measurements is due to the fact that the temperature is essentially a logarithmic function of the variables E_λ, a and ε.

4.2.2 LBL-NASA* Technique

Measuring Principle

Figure 6 shows the experimental set-up [45]. The UO_2 target is heated with a Nd-glass laser ($\lambda = 1.06 \mu\text{m}$) at an ambient gas pressure of 3 kPa. The generated UO_2 vapor expands into the ambient gas reaching supersonic velocities within the first .1 mm. However, collisions with the gas atoms force the vapor velocity again below Mach 1 at some distance x downstream. At this location a characteristic standing shock wave -- the Mach Disk -- becomes visible, caused by de-excitation of vapor molecules. The distance between laser crater and Mach Disk is recorded photographically. A silicon photodetector pyrometer serves for measuring the temperature in the evaporating crater.

Data Evaluation and Results

It was found both experimentally and theoretically that in free gasdynamic expansion from a gas reservoir, the location of the Mach-Disk can be described by

$$\frac{x}{d} = c \left(\frac{p_0}{p_1} \right)^{1/2} \quad \text{with } c \approx .67 \quad (26)$$

Here p_0 is the gas pressure in the reservoir and p_1 is the external pressure on the other side of the expansion orifice. Equation (26) was applied to the laser induced UO_2 vaporization, using the following analogies [46]:

*Lawrence Berkeley Laboratory/NASA Ames Research Center.

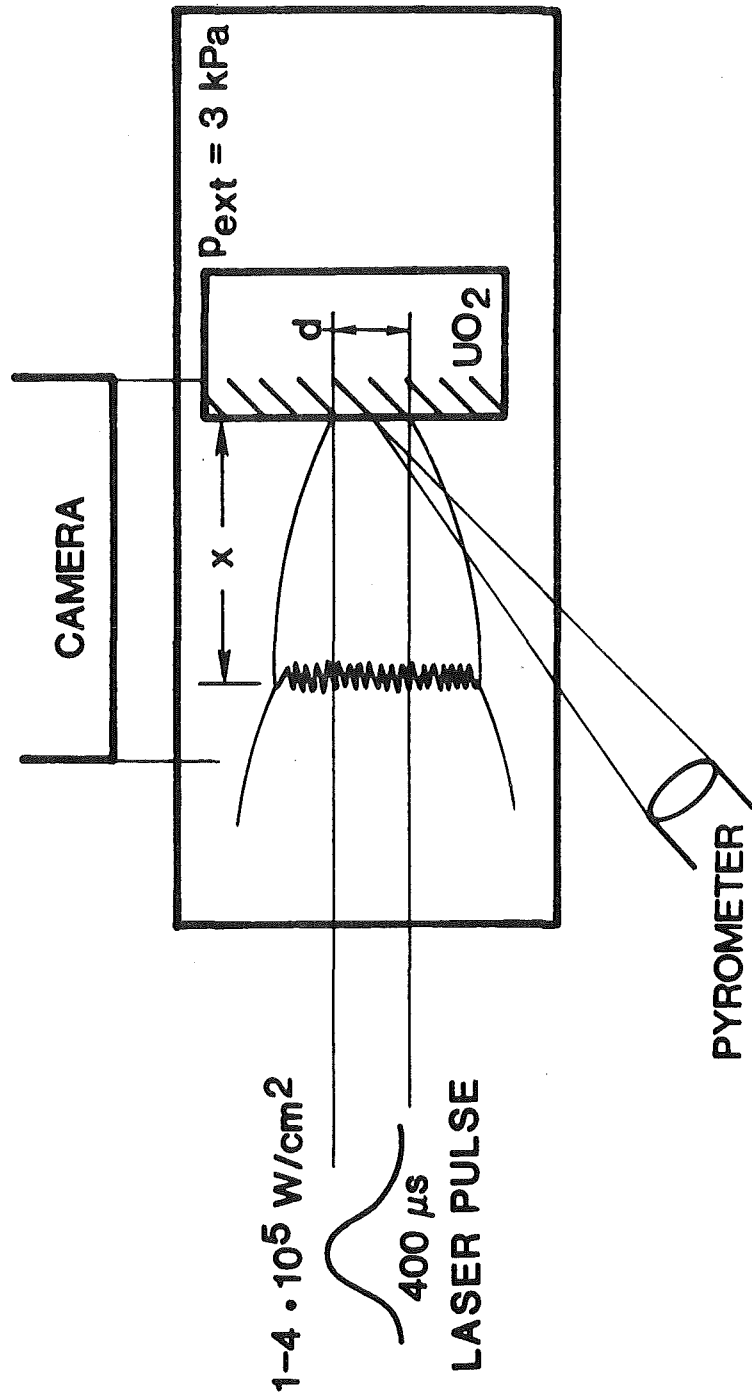


Figure 6. LBL-NASA Laser Heating Technique (Mach-Disk Method)

- o Orifice diameter d is the diameter of the laser crater,
and
- o reservoir pressure p_0 is the UO_2 saturation vapor pressure
at the maximum crater temperature.

The data points obtained for UO_2 are shown in Figure 4.

Evaluation of Method

The Mach Disk method for measuring the vapor pressure in laser evaporation was developed by Lovington et al. [47], who used it to measure the vapor pressure of carbon up to 4500 K. Since the results were in good agreement with calculated equilibrium vapor pressures, they suggested that the Mach-Disk method might be a new, useful way of determining saturation vapor pressures of refractory materials, provided further evidence could be gathered for the vaporization pressure actually being an equilibrium quantity.

The Mach-Disk results for UO_2 however turned out to be unexpectedly low (Figure 4).

The authors suspected contributions to this discrepancy from both temperature and pressure evaluation [45]:

- The measured crater temperatures could be too high due to the infrared emission of excited UO , UO_2 or UO_3 vapor molecules which would be detected by the wide band pyrometer, and
- interpretation of the whole visible laser spot as sonic orifice may overestimate d and underestimate p_0 , because Eq. (26) is based on a uniform pressure in the sonic

orifice, whereas the pressure in the laser crater does decrease in radial direction.

The first problem can be overcome by using an optical pyrometer, and the succeeding work followed this direction [48,49]. The results seem to essentially confirm the original temperature measurement so that the proper value for d in Eq. (26) remains the main question. However, the definition of a more appropriate "effective" orifice size d , is not immediately obvious. It requires a sound understanding of the gas-dynamic phenomena for both the reservoir expansion and the laser evaporation, and is directly coupled to the fundamental problem, to what extent Eq. (26) is applicable to laser induced vaporization. Present work at LBL aims at developing a broader theoretical basis for the Mach-Disk method.

4.2.3 ITU* Techniques

Two laser evaporation techniques were applied by the ITU group, firstly, free evaporation into vacuum [50,51], and secondly a modification of the Mach-Disk method [52]. Both approaches will be outlined below.

4.2.3.1 Vacuum Evaporation

Measuring Principle

A UO_2 sample is heated with 50 to 200 μs long pulses from a neodymium laser, typical crater diameter being 2 mm (Figure 7). The central crater temperature can be monitored with a

*European Institute for Transuranium Elements, Karlsruhe, FRG

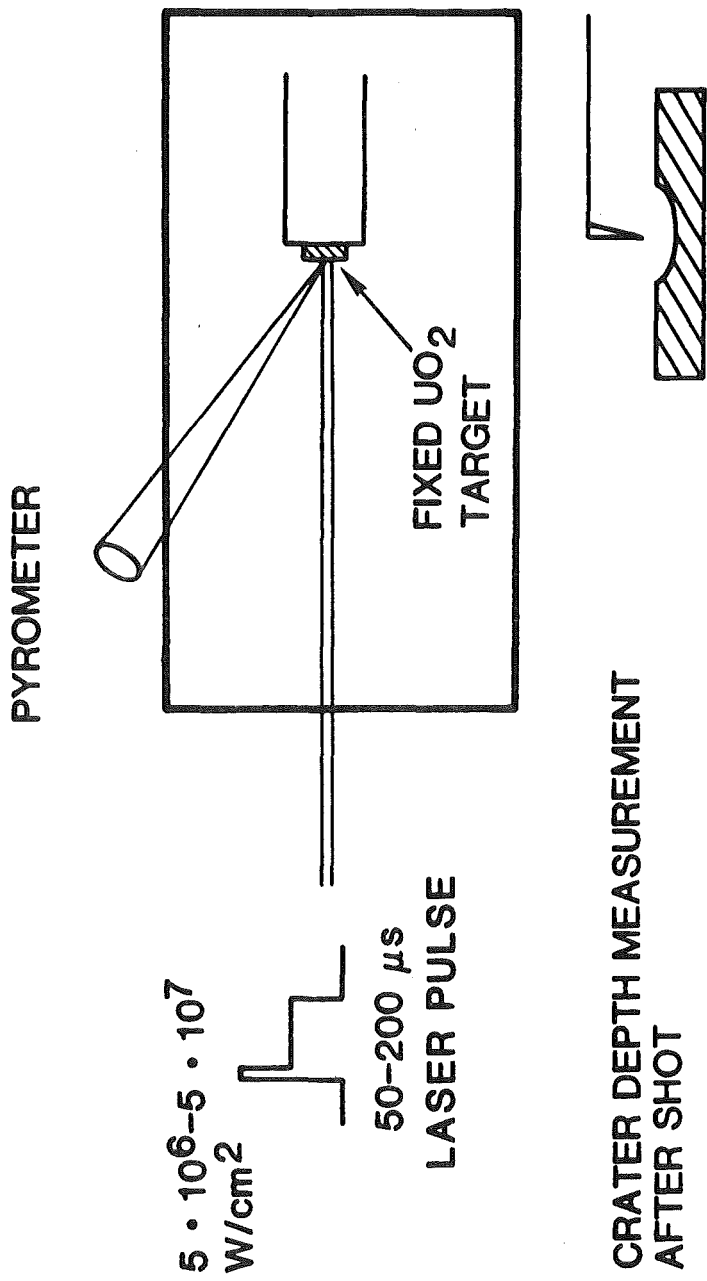


Figure 7. ITU Laser Heating Technique (Vacuum Evaporation)

pyrometer at several different wave lengths. For the temperature evaluation $\lambda = .65 \mu\text{m}$ is used.

After the experiment the central crater depth d is measured with an inductive sensor technique.

Data Evaluation and Results

The saturation vapor pressure p_{sat} is evaluated from the Hertz-Knudsen Equation

$$\frac{1}{A} \cdot \frac{dm}{dt} = \alpha_v p_{\text{sat}} (M/2\pi RT)^{1/2} \quad (27)$$

Under steady state conditions the evaporation rate per unit area follows from

$$\frac{1}{A} \cdot \frac{dm}{dt} = \rho_f \cdot \frac{d}{\Delta t} \quad (28)$$

With measured crater depth d , steady state evaporation time Δt , solid fuel density ρ_f , and assuming $\alpha_v = 1$, a vapor pressure is obtained from Eqs. (27) and (28). This pressure is then related to the pyrometrically measured temperature of the crater center. The published results for UO_2 are summarized in Figure 4.

Individual pressure and temperature uncertainties in the ITU-technique were not given, instead two lines bounding the experimental points were presented as an uncertainty estimate [51].

Evaluation of Method

The evaluation of pressure uncertainties in this technique requires some comments about Eqs. (27) and (28).

Eq. (27) assumes that the evaporation rate of a substance into vacuum ($dm/dt/A$) can be expressed by the kinetic theory expression for the number of molecules striking a unit area in unit time ($p_{\text{sat}} (M/2\pi RT)^{1/2}$), where p_{sat} is the equilibrium vapor pressure of the substance. Generally this relation is not obeyed, measured evaporation rates being smaller than predicted in this way. It became customary to lump all deviations from the above assumption into one empirical vaporization coefficient, or in other words, an empirical fudge factor was introduced to produce agreement between measured evaporation rates into vacuum and calculated kinetic theory expressions. It is important to realize that Eq. (27) is based on an unproven hypothesis, which lacks a rigorous deduction [53]. The way Eq. (27) is used here, it contains two unknowns, the equilibrium vapor pressure p_{sat} and the α_v which would be appropriate for the conditions of laser evaporation. There is no obvious way for determining it; only arbitrary assumptions can be made and $\alpha_v = 1$ was chosen in the pressure evaluation. Besides, the unsatisfactory physical content of Eq. (27) is demonstrated by the fact that it contains neither a property of the evaporating surface nor a property of the off-streaming non-equilibrium vapor phase. In the author's opinion, Eq. (27) is not relevant for the conditions of laser induced vaporization.

In this context another point about Eq. (27) needs clarification. Gas kinetic calculations for the problem of intensive evaporation into vacuum showed that -- in the case of a monatomic vapor -- the net evaporation rate is about 80%

of that given by Eq. (27) [54,55,56]. However, these calculations start from Eq. (27), using it as the source term for the number of molecules emitted from the surface. Consequently, these calculations do not support the applicability of Eq. (27), as was concluded in [57]. All they indicate is that in the evaporation regime with collision dominated vapor flux, approximately 20% of the emitted vapor atoms return to the surface, whatever the number of originally emitted atoms might be.

The second aspect of pressure evaluation in the ITU technique which needs some comments, is use of the crater depth as measure for the evaporation rate [Eq. (28)]. The implicit assumption here is that no liquid fuel is being pushed out of the crater by vapor recoil forces. Indeed, liquid layer displacement is a known phenomenon in laser vaporization [49,58] which is also observed in ITU experiments [59,60]. First it was reported that this problem could be overcome experimentally with a double pulse technique, in which a preceding short pulse with very high power density heats the UO_2 very quickly to the desired temperature level [61]. No liquid displacement was observed in the crater with this heating technique. Later model calculations predicted that liquid displacement is always present as long as a liquid layer exists in the crater [60], but it was argued that this effect would not be important in the crater center, only at its periphery. This conclusion is not very obvious if one considers the magnitude of the calculated radial flow velocities; given

For a typical surface recession velocity of $u = 1$ m/s and a liquid layer thickness $h = 2.5$ μm , the model predicts that liquid UO_2 leaves the innermost region of the crater surface of radius $r = .1$ mm with a radial velocity V_r of about 30 m/s or 3 mm during a measuring time of 100 μs .

A final comment on the pressure measurement concerns the mode of evaporation. If one compares the steady-state laser power density measured for a given fuel temperature in the ITU technique [97, Fig. 2] with that of the KfK-INR and LBL techniques, the former one is larger by 2-1/2 to 1-1/2 orders of magnitude ($T = 3500 \dots 4700$ K). A possible explanation for this discrepancy is, that the initial, very intense laser pulse in the ITU technique ($5 \cdot 10^7$ W/cm²) creates a plasma layer above the UO_2 surface which absorbs the energy of the second pulse. The UO_2 surface is then only heated indirectly by radiation, conduction and/or electron bombardment from the plasma layer. The material removal processes under such conditions are very complex. Indeed, the author was told* that no frozen liquid could be detected in 50 times magnified cross sections of the ITU crater centers after the experiments. (Assuming that frozen liquid should be visible as amorphous or very small grain structure.) Such frozen liquid is clearly visible in the other laser techniques [Ref. 41, Fig. 9 and Ref. 48, Fig. 3].

In the author's opinion, this fact and the apparent dissipation of energy in the ITU heating technique are strong evidence that the active evaporation mechanism differs from the purely phonon driven evaporation, which is of interest for HCDA purposes.

*P.R. Kinsman, Safety and Reliability Directorate, UK

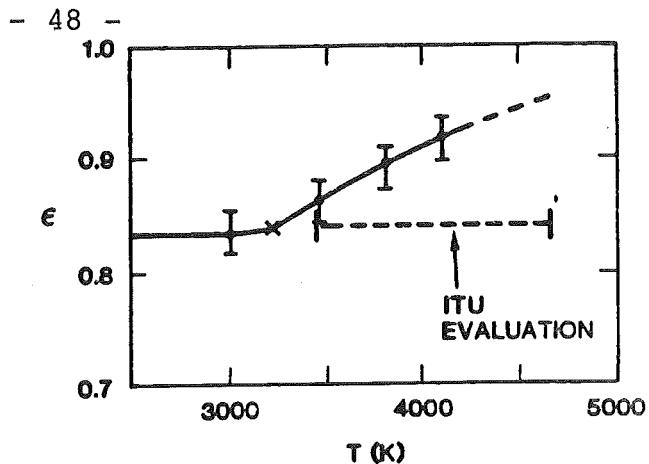


Figure 8.

Measured Emissivities of UO_2
and Data Used in the ITU
Temperature Evaluation.

I [43]
x [51]

The temperature uncertainties in the ITU technique are governed by Eqs. (25a-c). As in the KfK-INR technique dE_λ/E_λ can be expected to be $\pm 2\%$. The absorption of thermal radiation in the UO_2 vapor plume was neglected -- as in the KfK-INR measurements.

A constant UO_2 emissivity of $\epsilon_{.65} = .84$ was used in the temperature evaluation [51]. As is obvious from a comparison with measured data which became available meanwhile (Figure 8), this leads to a systematic temperature error. The data points around 4000 K should be shifted to lower temperatures by about 1.4%. The emissivity above 4200 K is not known. If it should follow the increasing trend, the data points at 4700 K in Figure 4 would be 2.9% too high in temperature. The random errors from uncertainties in E_λ and measured ϵ values combine to about $\pm .5\%$ in the temperature evaluation.

4.2.3.2 Modified Mach Disk Method

As already outlined in section 4.2.2, the measured quantities in this technique are Mach Disk location x , crater diameter d and external gas pressure p_{ext} . The main effort of the ITU group concentrated on deriving an improved evaluation model for the Mach Disk method [52]. This model was then

applied to laser vaporization of UO_2 .

Data Evaluation and Results

Starting from the original Mach Disk relation for the reservoir expansion [Eq. (26)]

$$p_0 = \frac{p_{\text{ext}}}{c^2} \left(\frac{x}{d} \right)^2 \quad (29)$$

the meaning of p_0 and d in the case of laser evaporation was investigated.

Both flows, that of the reservoir gas expansion and that of the laser induced vaporization, are considered identical beyond the first sonic point. By theoretically relating the pressure at this sonic point to either the reservoir pressure p_0 or to the vaporization pressure at the laser heated surface, p_{sur} , a connection is made between p_0 in Eq. (29) and the actually wanted p_{sur} . The result is

$$p_0 = A \cdot p_{\text{sur}} \quad \text{with } A = .42 \text{ to } .49 \quad (30)$$

$A = .45$ was used in the UO_2 data evaluation.

The orifice diameter d in Eq. (29) needs to be redefined for the laser case because a strong radial decrease of the pressure exists within the laser crater, while Eq. (29) was actually derived under the assumption of a radially constant pressure in the sonic orifice. For this purpose, the Euler flow equations for a cylindrically symmetric, adiabatic and supersonic flow were solved numerically, assuming as initial condition at the sonic plane a one-dimensional flow with radial

pressure variation. By matching the calculated relative axial density profile in the jet to the relative density profile from a uniform pressure source, a factor δ was obtained which is used to convert the diameter of the laser crater (d_m) to the gas dynamically appropriate diameter d in Eq. (21):

$$d = \delta \cdot d_m \quad \text{with } \delta = .45 \text{ to } .48 \text{ at } 4000 \text{ K} \quad (31) \\ = .37 \text{ to } .40 \text{ at } 5000 \text{ K}$$

The relation for the surface pressure p_{sur} at the crater center then reads:

$$p_{sur} = \frac{p_{ext}}{AC^2} \left(\frac{x}{\delta \cdot d_m} \right)^2 \quad (32)$$

The corresponding temperature in the crater center is measured by optical pyrometry. As the light emitted from the barrel shock wave and the Mach Disk disturbed the pyrometer signal above 4500 K, this was considered the upper practical limit for the temperature measurements. The associated uncertainty was estimated to $\leq \pm 1\%$. The quoted pressure uncertainties in this technique are indicated in Figure 4 for one data point.

Evaluation of Method

The pressure evaluation via Eq. (32) depends on experimental quantities (p_{ext} , x , d_m) and calculated factors (A , δ). Among the experimental quantities mainly the diameter of the molten region d_m seems uncertain because its actual size can be obscured by traverse heat conduction and radial displacement of molten material. The last effect was previously identified by the ITU group to be especially severe in the outer crater

region [60], but its impact on determining d_m in this technique is not discussed.

The modifying factor $1/(A \cdot \delta^2)$ which was introduced into Eq. (29) to yield Eq. (32), relies on complicated gas dynamic calculations. Moreover this modification -- which amounts to a factor of 10 -- essentially controls the final pressure result. Consequently, the uncertainties in A and especially δ govern the precision of the whole technique. While definition of A requires a correct treatment of gas dynamic phenomena before the first sonic plane, δ follows from modelling the gas expansion downstream of this sonic plane. Calculations of both flow regimes are extremely difficult and were only attempted so far for a monatomic gas of one-dimensional flow structure, combined with simplified initial and boundary conditions. Several important characteristics of UO_2 vapor are ignored in these calculations:

- UO_2 vapor is a multicomponent mixture,
- not only translational but also internal degrees of freedoms relax during the vapor expansion, and
- translational cooling during the vapor expansion leads to significant vapor supersaturation which can cause UO_2 condensation (the kinetics should be fast enough).

Mainly, the last two effects, which can feed considerable additional energy into the expansion flow, must be expected to have a noticeable influence on the vapor flow structure and thus on A and δ . (At 4000 K the heat of vaporization

corresponds to about 30 degrees of freedom!) The possible non-adiabaticity of UO_2 vapor flow may destroy the analogy between reservoir expansion and laser induced evaporation on which the Mach Disk method is based. Clearly further work is needed to secure the theoretical basis developed so far for this method.

4.2.4 MAP* Technique

The MAP technique [62] involves laser heating of UO_2 with power densities up to $5 \cdot 10^{10}$ W/cm². Only two p-T points obtained with this technique have been published, indicating about 240 MPa at 8000 K and 1040 MPa at 10,000 K. Because experiment interpretation is very difficult and because the experiment conditions are far away from any conceivable HCDA situation, the MAP results were not included in Figure 4. The measured pressures lie roughly one decade above the extrapolated IAEA standard, possibly indicating that the material state was no longer on the saturation line but in the supercritical region.

4.3 Assessment of Experimental p(T) results

As outlined in Section 2, the goal is to identify the factor-of-4 (or 2) pressure band which contains the true saturation vapor pressure of UO_2 without doubt. This section will first summarize the accomplishments of the various techniques in the light of this goal. Then the remaining open questions which are common to all laser vaporization techniques will be discussed.

*Mitsubishi Atomic Power, Japan

4.3.1 Transpiration Technique

Although the transpiration results extend only a few hundred degrees into the liquid range, they appear to be very valuable data points for the following reasons:

- The results for solid UO_2 agree well with those of other techniques, indicating that the important requirements of the transpiration method, e.g., carrier gas saturation, were met.
- The evaporation conditions are very similar to those expected in HCDA situations, in the sense that the liquid-vapor mass transfer is solely driven by equilibrium energy transfer from phonons to surface atoms.
- Combination of pressure uncertainties ($\pm 10\%$) and temperature uncertainties ($\pm 1\%$) lead to a pressure band which is within the factor-of-2 goal.

In summary, the transpiration data deserve a high weight in the overall picture of Figure 4.

4.3.2 KfK-INR Technique

The pressure evaluation model addresses the main gas-dynamic features of the free vapor expansion encountered in laser induced UO_2 vaporization. It was concluded in section 4.2.1 that the combined pressure uncertainty from random and systematic errors could be somewhat larger than a factor of

The temperature uncertainty in the first series was relatively large ($\pm 6\%$) mainly due to uncertainties in the number of

relaxing degrees of freedom. The later measurements used optical pyrometry, based on UO_2 emissivities which were measured by the same group with the same pyrometry technique. The resulting temperature uncertainty was estimated to less than $\pm 1\%$.

So apart from the below discussed problem of optical absorption in laser evaporation, it appears that the KfK-INR technique is a valid approach for measuring the laser induced vapor pressure of UO_{2-x} . The achieved degree of uncertainty corresponds roughly to the factor-of-4 goal, defined in section 2.

4.3.3 LBL-NASA Technique

The first Mach Disk results for UO_2 must be considered preliminary until the phenomena involved are fully understood. Most importantly, a more appropriate and convincing redefinition of the effective orifice diameter d for the case of laser induced evaporation is needed. The present work at LBL addresses in a very consequent way the most important aspects of the Mach Disk method:

- The coupled heat and mass transfer in the evaporating UO_2 surface, including composition changes [63],
- gas kinetic calculations for the various flow regimes in the vapor plume [64], and
- mass spectrometric investigations of the vapor cloud composition [65].

These efforts will probably allow an improved re-interpretation of the first measurement series and will contribute to the further development of the Mach Disk method.

4.3.4 ITU Vacuum Evaporation

The pressure evaluation in this technique is based on a relation which -- in the author's opinion -- has no physical relevance for the conditions encountered in laser induced evaporation (section 4.2.3.1). Its formal application to laser evaporation may result in significant errors, but a reliable estimate is not possible at the present time.

With respect to the pyrometric temperature measurement, a systematic correction of the temperatures seems necessary since a constant UO_2 emissivity of $\epsilon_{.65} = .84$ was used in the evaluation. The emissivity data, which became available meanwhile, indicate that the temperatures plotted in Figure 4 should be about 2% lower at 4200 K and probably 3% lower at 4700 K.

In the author's opinion, significant unresolved uncertainty margins are still associated with the ITU pressure evaluation, making it infeasible to assign an overall uncertainty estimate to these p-T data.

4.3.5 ITU Mach Disk Method

The ITU group redefined reservoir pressure p_0 and sonic orifice diameter d of the original Mach Disk approach on the basis of a gas dynamic analogy. Since the modifying constant for the derived vapor pressure is large -- a factor of 9 to 11 -- the error margins in the ITU Mach Disk method are governed by the accuracy with which the modifying constant $(1/(A \cdot \delta^2))$ is known. Although the gas dynamic calculations done so far largely extended the theoretical basis for this technique,

it appears that important characteristics of UO_2 vapor, like internal degrees of freedom and vapor condensation, were neglected. Further work must show if the constructed gas dynamic analogy between reservoir expansion and laser induced vaporization is compatible with these properties of UO_2 vapor and if so, what their influence on the calculated values for A and δ is. The published pressure uncertainty of a factor 2.5 (see Figure 4) may or may not cover the effects from ignored UO_2 vapor properties.

4.3.6 Open Questions in Laser Evaporation

Aside from the above discussed uncertainties in the individual laser results, three open questions exist with all laser techniques. Answers to these questions will be needed before a final assessment of the laser results and their significance for HCDA conditions can be made.

4.3.6.1 Optical Absorption in UO_2 Vapor

A common problem of the pyrometric temperature measurement is that light emanating from the laser crater could be absorbed in the UO_2 vapor plume. This question was investigated in some detail by both the KfK-INR and the ITU group [18,57]. In [18] it was concluded that equilibrium UO_2 vapor quickly becomes opaque at temperatures above 4000 K due to bound-bound transitions in the electron shells of the vapor molecules. In [57] the result was that optical pyrometry should be possible up to a UO_2 surface temperature of 6000 K, mainly because it was assumed that optical absorption is determined by the

thermally produced free electrons and that 6000 K vapor cools rapidly down to 4000 K during its expansion into vacuum.

Both investigations do not fully address the conditions of interest because optical absorption is not determined by the translational temperature of the vapor molecules but rather by their electronic temperature. Important for the actual absorption are therefore

- the electronic temperature of the laser generated vapor molecules as they leave the liquid-vapor interface, and
- the relaxation of this electronic temperature during vapor expansion.

Since the electronic temperature is probably governed by collisions with the free electron gas in the vapor cloud, vapor ionization by the incident laser light might become important. This effect was observed in similar laser experiments [66]. Thus the optical absorption in laser induced UO_2 vapor can probably only be quantified with the necessary precision by performing transmission experiments on UO_2 vapor clouds, as proposed in [18].

Optical absorption was neglected in all laser experiments on UO_2 . Eq. (25b) predicts that an absorption of 10% at 4000 K would result in a temperature which is 2% too low. The ITU temperatures are much more vulnerable to optical absorption than the KfK-INR temperatures because beam and crater diameter are about 10 times larger.

4.3.6.2 Composition Changes in the Evaporating Surface

Since UO_2 generally evaporates incongruently, composition changes in the evaporating surface are to be expected. This effect, which may imply vapor pressure changes, must be understood for the complete interpretation of laser results.

A model for the surface changes [67] predicts for UO_2 that the surface composition converges against that composition at which the off-streaming vapor has an overall O/U-ratio of exactly 2.00. If one assumes the equilibrium vapor composition to exist at the liquid-vapor interphase, the surface becomes increasingly substoichiometric with temperatures, e.g., $\text{UO}_{1.70}$ at 4500 K. Calculated equilibrium vapor pressures of such substoichiometric oxides depend only weakly on the O/U ratio, so that in the first approximation surface changes can be neglected up to 4500 K. Similar calculations with other thermodynamic input data confirmed this conclusion [68].

However, if thermodynamic equilibrium should not be present at the liquid-vapor interphase, the extent of surface changes and their consequences on vapor pressures is again an open question.

Investigations on zirconium hydride -- which has a fluorite structure like UO_2 -- revealed that the evaporating H and H_2 was in thermal equilibrium with the surface (Maxwell velocity distribution) but not in chemical equilibrium with itself (H/ H_2 ratio) nor with the composition of the evaporating surface [69].

In the light of these results similar investigations for UO_2 appear necessary before the effect of surface changes on laser vapor pressures can be established without doubt.

4.3.6.3 Laser Induced Evaporation

The third point which needs clarification, concerns the evaporation mechanism that is active in laser induced evaporation. This important question was only recently addressed by the ITU group which investigated the energy transfer under laser heating conditions. As indicated below, the incoming laser photons are absorbed by electrons and their energy is then passed on through the various statistical subsystems [52]:

photons \rightleftharpoons electrons \rightleftharpoons phonons \rightleftharpoons surface atoms \rightleftharpoons vapor

Conclusions for the behavior of these coupled systems under the extreme conditions of high intensity laser radiation were not yet published. However, the responsible authors feel that -- aside from phonon induced liquid-vapor mass transfer -- mechanisms like multiphoton/surface-atom or electron/surface-atom interactions cause additional material removal from the surface [70]. The mass spectrometric results in zirconium hydride [69] indeed seem to indicate the presence of some non-equilibrium evaporation processes. Therefore, the microscopic, multi-step evaporation process acting in laser vaporization must be understood before the significance of laser induced vapor pressures for HCDA situations can be evaluated.

4.3.7 Summary

The quite precise transpiration data -- which have a pressure uncertainty factor $p/p_0 < 2$ -- indicate a saturation vapor pressure slightly below the IAEA standard (Figure 4). Unfortunately, these data extend only to 3400 K.

At higher temperatures only laser results are available. From this assessment of the pressure and temperature evaluation in the various laser techniques, it appears that the overall pressure uncertainty factor p/p_0 is either greater than 4 or close to 4 (KfK-INR technique) mainly due to uncertainties in the pressure evaluation. Little uncertainties result in principle from the pyrometric temperature measurement, provided correct UO_2 emissivities are used. However, in addition to these experiment-related uncertainties, three open questions remain, which must be answered before a final assessment of the laser results can be made:

- Is optical absorption of the light emanating from the laser crater indeed negligible, as was assumed in all pyrometric temperature measurements?
- What is the effect of surface composition changes in the laser crater ($UO_2 \rightarrow UO_{2-x}$) on the measured vapor pressure?
- Is a laser induced vapor pressure really a true equilibrium vapor pressure or exist additional material removal processes under the conditions of intense laser evaporation?

At present -- with these questions unanswered -- the measured vapor pressure data above 3400 K remain very uncertain and their significance for HCDA calculations, which require equilibrium data, is unclear.

4.4 Fission Heating

4.4.1 SNL* Technique

Measuring Principle

A flat disk of $\text{UO}_{2.08}$ with a mass of about 1 g (Figure 9) is fission-heated to a desired maximum temperature, or energy, within 10 ms [71,72]. The evolving transient fuel vapor pressure is measured with a pressure transducer. Six thermocouples are located in the graphite crucible in order to evaluate time dependent heat losses from the fuel sample to the surrounding walls. During an experiment the following signals are recorded:

- Cell pressure $p(t)$ from pressure transducer,
- Relative reactor power $P(t)$ from in-pile neutron detector
- Starting time and end of reactor pulse (t_0 and t_E) from ion chamber outside reactor core, and
- Temperatures $T(t)$ in graphite walls from thermocouples.

After the experiment the total fission energy deposited in the sample U_{tot} is determined with fission product inventory analysis.

Data Evaluation and Results

Besides the original data evaluation [71] a refined analysis of the measured results was undertaken [73].

*Sandia National Laboratories, Albuquerque, New Mexico

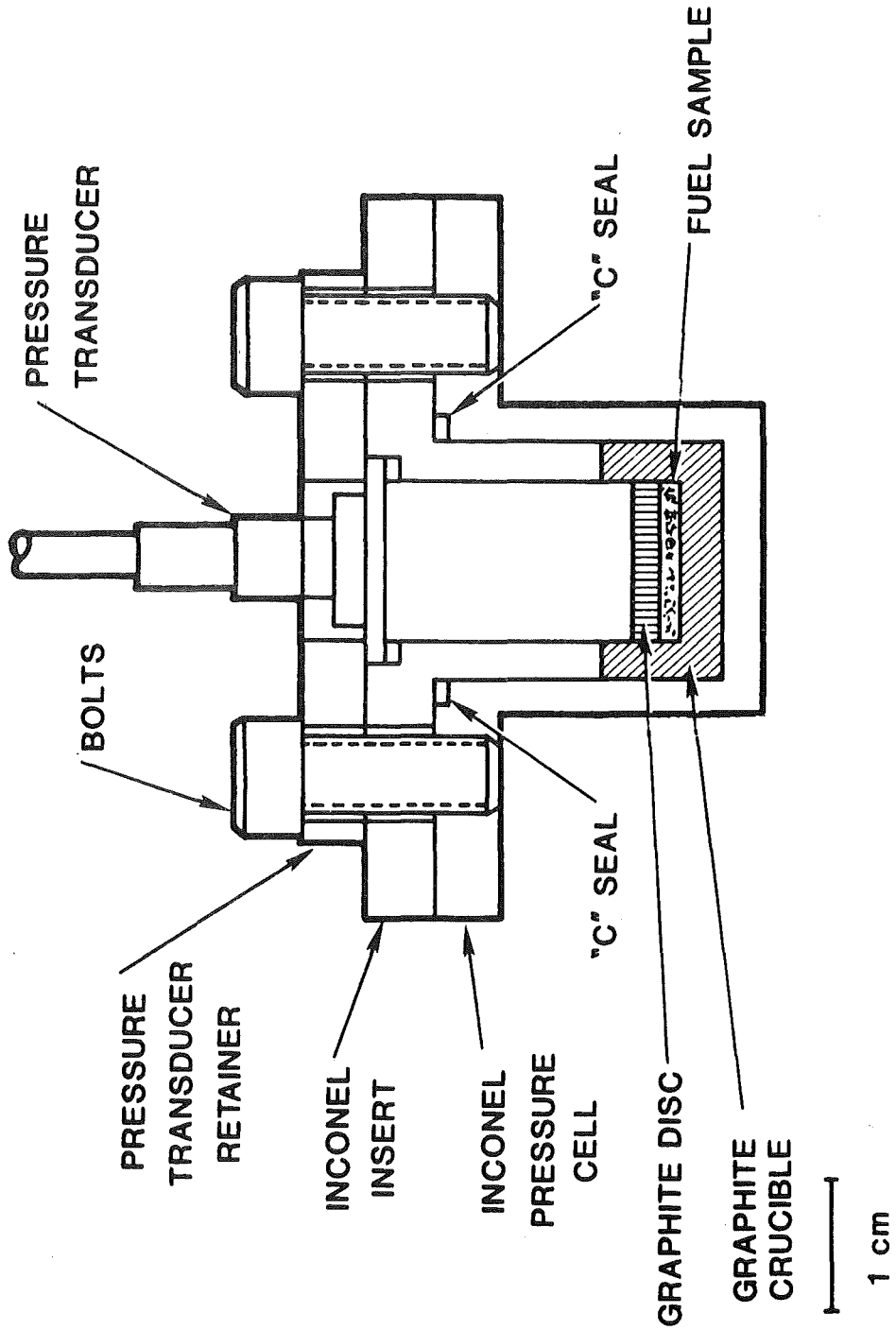


Figure 9. SNL Fission Heating Technique

To allow a unified description of these analyses, first the general evaluation procedure and then the different specific approaches will be outlined below.

Closed-volume in-pile experiments are subject to the following important phenomena which must be treated in any analysis:

- Loss of initial fuel geometry caused by movement of liquid fuel within the available free volume,
- Neutronic energy deposition changes in the moving fuel due to changing neutronic self-shielding, and
- Heat transfer to the surrounding walls.

Aim of the analysis is to calculate an upper and a lower bound for the internal fuel energy $U(t)$ which corresponds to the pressure $p(t)$ measured at a given time. A convenient lower bound for $U(t)$ is the volumetric average energy $U_{avg}(t)$ deposited in the sample at time t . U_{avg} would be the relevant driving energy if total thermal mixing occurred during the experiment. (Heat losses are neglected for a moment). The volumetric average energy can be written as

$$U_{avg}(t) = U_{tot} \cdot \frac{\int_{t_0}^t CF(t) \cdot P(t) dt}{\int_{t_0}^{t_E} CF(t) \cdot P(t) dt} \quad (33)$$

where CF is the volumetrically averaged coupling factor of the UO_2 sample ($W/gUO_2/MW$ reactor power). An appropriate upper bound for the fuel energy at time t is the peak energy $U_{pk}(t)$ deposited in the sample. U_{pk} would be the relevant fuel energy if no thermal mixing occurred during the experiment. The peak energy follows from

$$U_{pk}(t) = U_{tot} \cdot \frac{\int_{t_0}^t PA(t) \cdot CF(t) \cdot P(t) dt}{\int_{t_0}^{t_E} CF(t) \cdot P(t) dt} \quad (34)$$

with $PA(t)$ = ratio of peak to average energy deposition in the sample at time t .

With heat losses included, U_{pk} is still an upper bound for the internal fuel energy. U_{avg} however is decreased by heat losses, but if these are restricted only to the outer fuel region close to the walls, Eq. (33) still gives a valid lower bound for the unaffected inner fuel region. With this requirement in mind, the above defined average and peak energies are two valid limits for the energy deposited at time t .

In Eqs. (33) and (34) the quantities U_{tot} , t_0 , t_E and $P(t)$ are measured while time dependent coupling factor $CF(t)$ and peak-to-average ratio $PA(t)$ need to be calculated. In the original data evaluation CF and PA were calculated for the

initial disk geometry with a S-4 version of the two-dimensional neutron transport code TWOTRAN [71]. These constant values were then used for analysis of the whole experiment (Figures 10a and b). Heat losses were neglected because the thermocouples in the graphite walls recorded only minor temperature increases during the pressure measuring times. Figure 11 shows the result of the original data evaluation.

In view of the simplifying assumptions in this first analysis a refined data evaluation followed [73]. Hydrodynamic calculations with CSQ-II, which has a fixed energy deposition grid, indicated violent dispersal of the fuel disk during and after fuel melting. As a result, the coupling factor increases and the peak-to-average ratio decreases. Figures 10a and b show the S-8 TWOTRAN results for the initial disk geometry and two dispersed fuel configurations, termed "shell" and "100% smeared" geometry, respectively. Since it was felt that these two dispersed geometries should bound the actual fuel dispersal, the step function pairs in Figure 10 a and b were used in the refined analysis. In addition complete thermal mixing was assumed at the time of dispersal. The resulting energy band in Figure 11 is quite similar to the original evaluation because some of the effects included in the refined analysis tend to cancel each other.

Evaluation of Method

The pressure is measured with a flexible membrane type transducer, the signal of which is determined by the travel

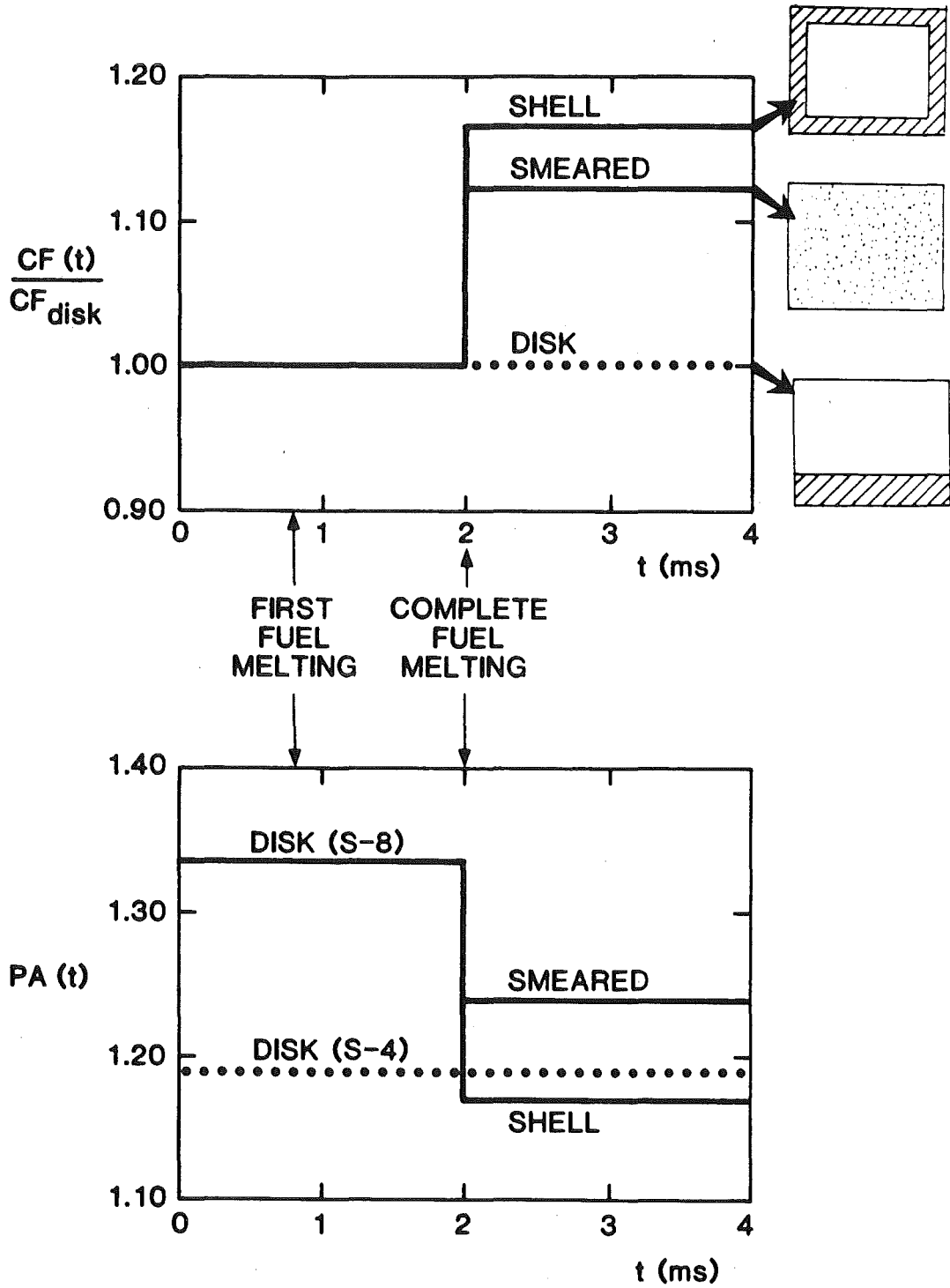


Figure 10a. Calculated neutronic coupling factors for different fuel geometries as used in the energy evaluation of [71](...) and of [73] (—).

10b. Calculated peak-to-average ratios of energy depositions into different fuel geometries as used in [71] and [73].

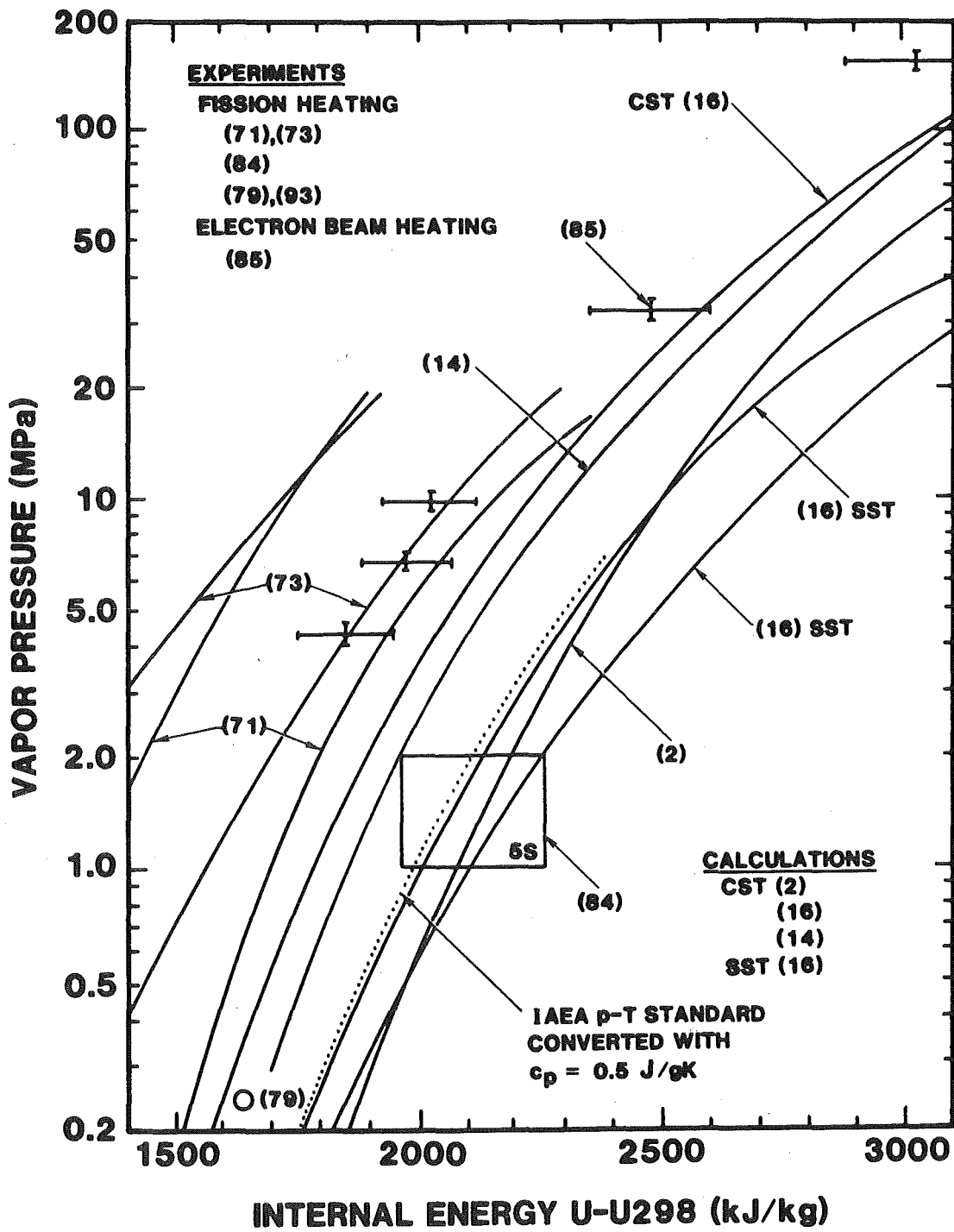


Figure 11. Measured and calculated saturation vapor pressures of liquid UO_2 as function of internal energy

of the center part of the membrane. The transducer is calibrated in a high pressure gas system under isobaric and isothermal conditions, which do not necessarily exist during the dynamic in-pile test. CSQ-II calculations indicated that pressure gradients along the transducer membrane should not be significant during in-pile tests [74].

Thermal gradients in the transducer membrane from hot material splashing against the membrane surface, turned out to be a more severe problem. Due to differential thermal expansion, the membrane tends to buckle inwards, giving rise to negative pressures. (In order to delay this effect, a 1 mm thick graphite disk was glued onto the Inconel membrane [71]). Later calculations however, indicated that even this configuration could give rise to 1 to 2 MPa of negative pressure during the experiment [75]. Early anomalies seen in measured pressure traces could support these theoretical results.

Another question which arises with respect to the pressure measurement is CO-formation from a C-UO₂ reaction. This possible pressure source could be eliminated on the basis of limited oxygen transport kinetics and additional inhibiting mechanisms, like the vapor deposited UO₂ liner seen on the graphite walls after the experiment [76,77].

A final aspect of the pressure measurement is fuel contamination [78]. Any fuel contaminant that evolves into a gaseous state during the fission heating will be detected by the pressure transducer. Two sources for contaminants must

be distinguished: impurities from the fabrication process (intrinsic contamination) and substances introduced during test preparation itself (extrinsic contamination). While the intrinsic impurities would also show up in a HCDA, the extrinsic impurities are non-prototypical and must be avoided. Since no special precautions were taken in the original SNL test preparation, some extrinsic contamination might have been introduced.

In summary, two not well quantified effects on the pressure measurement remain: membrane buckling and extrinsic impurities. Although these effects have a canceling tendency, the author's personal feeling is that impurities could have prevailed, provided the release kinetics were fast enough.

The energy bands shown in Figure 11 do not include random errors from input data. These random errors -- as well as possible systematic deviations -- will now be estimated from Eqs. (33) and (34).

The average internal energy U_{avg} is insensitive to changes in $P(t)$ or $CF(t)$ since they both appear in numerator and denominator of Eq. (33). A complete error analysis of Eq. (33) shows that a 20% change in $CF(t)$ for $t > t_{melt}$ translates into only a few percent change in $U_{avg}(t)$. The same insensitivity exists for changes in $P(t)$. The uncertainty in U_{tot} which is estimated to $\pm 5\%$, enters fully so that the random error in the average internal energy U_{avg} is

$$\delta U_{avg}/U_{avg} \approx \delta U_{tot}/U_{tot} \approx \pm 5\% \quad (35)$$

With respect to the peak internal energy [Eq. (34)] the same uncertainties enter from U_{tot} , CF and P. The additional uncertainty from PA ($\pm 5\%$) enters fully and the random uncertainty for U_{pk} can be estimated as:

$$\delta U_{pk}/U_{pk} \approx \left[(\delta U_{avg}/U_{avg})^2 + (\delta PA/PA)^2 \right]^{1/2} \approx \pm 7\% \quad (35)$$

Eqs. (35) and (36) show that it is most important for an exact energy evaluation to know U_{tot} and PA as precise as possible.

Aside from the above discussed random errors in U_{avg} and U_{pk} , there might also exist a systematic error. Recent modeling efforts with an interactive code system (CSQ-TWOTRAN), which allows a recalculation of the neutronic energy deposition as the liquid fuel changes its geometry, did not confirm the earlier CSQ results of a dispersive fuel motion. Rather a compaction of the initial flat disk into a column-like structure is obtained [74]. Since this is a neutronicly denser fuel configuration than the flat disk, the coupling factor decreases (to about .95 in Figure 10a) and the peak-to-average ratio increases (to about 1.40 in Figure 10b). Since U_{avg} is very insensitive to changes in $CF(t)$, the question of liquid fuel geometry -- dispersed or compacted -- has little effect on the calculated value of $U_{avg}(t)$. However, in the case of U_{pk} , the question of liquid fuel geometry is of importance, because PA enters linearly in Eq. (34). If the compacted geometry is attained in the liquid state, the peak energy deposition is about 20% higher than the line calculated in

[73]. Thus, U_{pk} depends strongly on the geometrical changes during the course of the experiment. (The conclusion for future measurements is to use as little fuel as possible without becoming too vulnerable to heat losses).

The Level I goal of $\pm 6\%$ in internal energy is clearly not reached in these first in-pile vapor pressure measurements. While the low energy bound is established within $\pm 5\%$, the peak energy can be too low by up to 20%, depending on the actual fuel geometry obtained in the liquid state.

4.4.2 CEA* Technique

Measuring Principle

A thin UO_2 disk (.3 mm thick, 7 mm diameter, 93% U-235) is fission heated in a tungsten tube containing .1 MPa of Ar gas [79]. The tube contains a pressure transducer and a condenser plate, the temperature of which can be monitored with a fast thermocouple (Figure 12). The ratio of free volume to fuel volume is 14. Typical heating times in the pulsed Silene reactor are 10 ms. For a $p(U)$ measurement, the following data are taken:

- The pressure $p(t)$
- The relative reactor power $P(t)$
- The temperature of the condenser plate,
and after the in-pile irradiation:
- The total number of fissions in the sample by fission product γ -counting.

*Commissariat à l'Énergie Atomique, Fontenay-aux-Roses, France

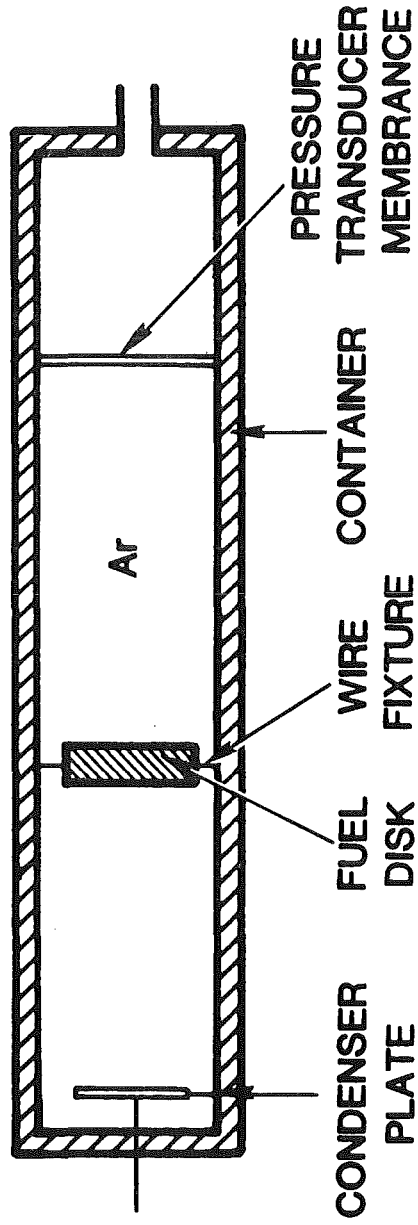


Figure 12. CEA Fission Heating Technique

Data Evaluation and Results

The pressure signal $p(t)$ is taken from the Argon filling gas in the capsule, far away from the UO_2 pressure source. Assuming that no pressure gradients existed between UO_2 surface and transducer, this uncorrected signal was interpreted as UO_2 vapor pressure in the original paper [79]. In the meantime the authors feel that pressure gradients develop in the off-streaming UO_2 vapor plume as the vapor pressure significantly exceeds that of the filling gas. Their new data evaluation identifies the point in time where a sudden pressure rise indicates fuel boiling; at that time the fuel vapor pressure equals the Argon gas pressure as recorded by the transducer shortly before onset of boiling [93].

The evaluation of the corresponding fuel average energy follows in principle Eq. (33). The total energy deposition U_{tot} in Eq. (33) is obtained by multiplying the measured total number of fissions in the sample with a measured value for the energy per fission of 170 MeV/fission. The fission rate in the fuel is assumed to be proportional to the reactor power, which is equivalent to a constant coupling factor CF . CF then cancels in Eq. (33). The result was 1650 J/g, which is related to a measured gas pressure at boiling onset of .235 MPa.

Evaluation of Method

The pressure evaluation is an application of the approved boiling point method for measuring vapor pressures of liquids. Some uncertainties exist in defining the onset of boiling because

the change in dP/dt is not very distinct. However, the resulting uncertainty for the pressure evaluation of about $\pm 20\%$ is well within the pressure goals defined in section 2.

Thermal bowing of the transducer membrane is not a problem here due to the extremely thin membrane in the used transducer (Kistler type). Early in the development of the CEA method, it became clear that extrinsic impurities -- mainly water and carbon -- were introduced during test preparation. With the aid of mass-spectrometric investigations on the post-test capsule atmosphere, the preparation route was developed to the stage where extrinsic impurities became insignificant. The pressure magnitudes seen in the CEA experiments can therefore be considered HCDA typical, including contributions from both fuel vapor and intrinsic fuel impurities. The precision in the pressure measurement appears to be around $\pm 20\%$, which is excellent.

The energy evaluation however is subject to random and systematic errors.

First, the above mentioned uncertainty in the boiling time translates into about $\pm 5\%$ in average fuel energy [79, Figure 2]. Secondly, U_{tot} in Eq. (33) is only known within another $\pm 5\%$. Thirdly, a systematic deviation arises from the fact that a constant coupling factor was used in deriving $U_{avg}(t)$. In reality, the coupling factor before dispersal ($t_0 \leq t \leq t_{boil}$) which enters in the numerator of Eq. (33) is different from the coupling factor in the denominator ($t_0 \leq t \leq t_E$) due to the fuel dispersal after boiling begin.

The author's rough guess from the coupling factors shown in Figure 10a and from Figure 2 in [79] is that the true average energy at time of boiling is 8% lower than the value derived in the CEA evaluation. An additional effect which is not taken into account is γ -heating. From scoping calculations done for the Annular Core Research Reactor at SNL [80], one could estimate that this increased U_{avg} by about 1 to 2%.

The prevailing systematic error with the energy evaluation however, is neglect of energy deposition gradients in the initial fuel disk. Since the characteristic quantity for neutron absorption $\Sigma^{U-235} \cdot x$ is the same for the CEA fuel disk (.3 mm thick, 93% U-235) as for the SNL fuel disk (.9 mm thick, 30% U-235), the peak-to-average ratios from Figure 10b may be used here as a first approximation. According to this figure, the surface energy deposition in the CEA-disk would be $1.34 \times U_{avg}$, boiling will however occur somewhat below the surface due to radiation losses. A rough estimate gives $PA = 1.20 \dots 1.25$ for the boiling zone. So in summary, the actual energy deposition in the boiling zone would be higher than the average energy deposition from the CEA evaluation method by

$$E_{boil} - E_{avg}^{CEA} = - 8\% + (1\dots2\%) + (20\dots25\%) = + 13\dots19\% ,$$

provided that the calculated data of Figure 10 are indeed representative for the CEA fuel. In any case, it appears that the energy evaluation in the initial CEA method [79]

is not on a Level I precision ($\pm 6\%$) because important effects are neglected in observing the energy deposition of the boiling fuel zone.

4.4.3 Integral Pin Tests

Quite a number of in-pile heating experiments on single fuel pins or pin bundles have been performed in several laboratories. In these integral tests, fission energy is deposited into the fuel and -- provided cladding failure occurs -- the pressure history in the surrounding sodium coolant channel is recorded. Although not the main goal of such tests, the pressure measured at time of clad failure contains information about the fuel pressure-energy relation.

In deriving this $p_{\text{sat}}-U$ information from integral pin tests, the following effects must be considered:

1. Heat losses from the pin prior to clad failure,
2. pressure in the pin from incondensable gases,
3. pressures from sodium vapor or fuel-coolant interactions after clad failure, and
4. acoustic phenomena in the transmitting sodium column.

With these effects separated, the peak energy deposition in the pin at failure time can in principle be related to the fuel vapor pressure at the same time. However, most difficult to quantify is the pressure contribution inside the pin from incondensable gases, like fill gas and intrinsic fuel impurities. Of the various single pin TOP-like experiments which were reviewed [81,82,83], only the test PBE-5S performed at Sandia

National Laboratories appears to be evaluable.

In this test [81] a single UO_2 pin was subjected to a single reactor pulse of about 5 ms width (FWHM). During the course of an intensive analysis of this test, it became clear that the measured pressures in the sodium could only be explained if significant amounts of incondensable gases were present at failure time [84]. In a parametric study, the optimum fit of the experimental pressure data was found with a gas content which is typical for normal fuel impurity levels and with the fuel vapor pressure shown in Figure 11. The corresponding fuel energy is the peak energy deposited in the pin at time of failure.

4.5 Electron Beam Heating

Uranium oxide samples were heated far into the liquid range by using the Relativistic Electron Beam Accelerator (REBA) at SNL [85].

Measuring Principle

Figure 13 gives a schematic sketch of the experimental setup. A thin layer of $\text{UO}_{2.08}$ powder is confined between two movable graphite pistons. After the sample is heated to a desired internal energy in about 1 μs , the evolving vapor accelerates the pistons in opposite directions. The piston motion is followed for the next 5 to 20 μs by recording the time dependent width of their shadows. A fast infrared pyrometer measures the total temperature rise in a graphite dosimeter plate. The graphite components in this experiment remain

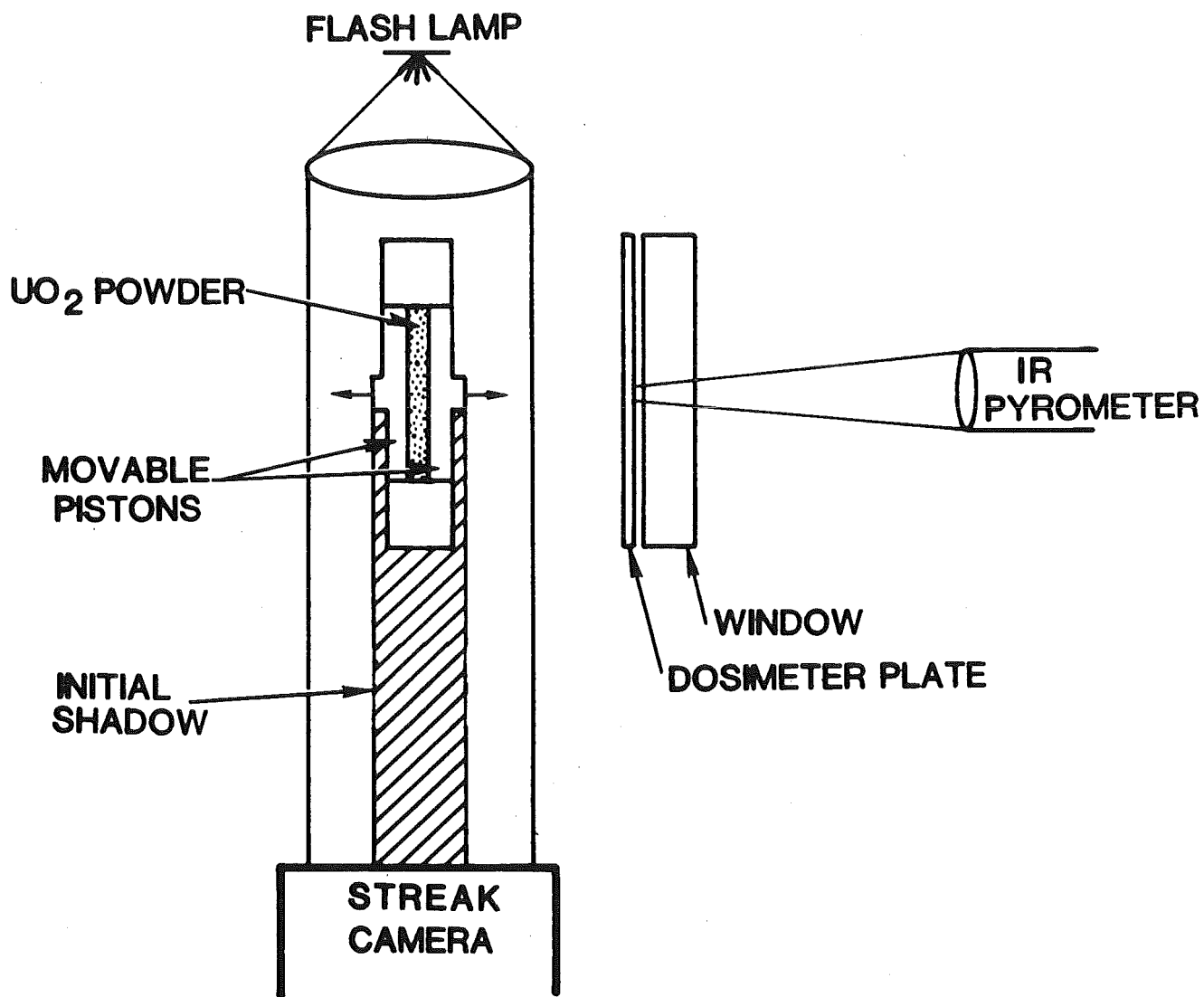


Figure 13. SNL Electron Beam Heating Technique

below 2300 K because of the large heat capacity of carbon (≈ 2 J/gK).

Data Evaluation and Results

The energy deposited in the liquid sample is evaluated in the following way. The measured temperature rise in the graphite dosimeter is converted to an absorbed energy density, based on the known enthalpy data of graphite. Then an electron transport code is used to convert the graphite energy deposition to that in the uranium oxide sample. Required input data are experiment geometry, electron beam data, and cross-sections for both UO_2 and C. The total uncertainty associated with this energy evaluation was estimated to $\pm 5\%$. The calculated energy deposition profile across the 25 μm thick sample varied by 10%.

For the vapor pressure evaluation, the expansion of the liquid-vapor fuel mixture is treated as isobaric. This is based on assumed thermal equilibrium in the two-phase mixture and neglectable heat losses to the surrounding graphite walls. In an isobaric expansion, the internal pressure acting on the movable piston can be evaluated from the measured piston location $x(t)$, using the simple equation of motion:

$$p = \frac{m}{A} \ddot{x}$$

The acceleration \ddot{x} is found as the slope of the linear $\dot{x}(t)$ -plot. The resulting pressure is then correlated to the calculated peak energy deposited in the condensed sample prior

to its expansion. The p-U data obtained this way are plotted in Figure 11.

Evaluation of Method

Determination of the sample energy involves essentially two steps: pyrometric measurement of the dosimeter energy deposition and theoretical extension of the calorimeter energy to that of the $\text{UO}_{2.08}$ sample. Both steps were developed to high accuracies in preceding work, remaining uncertainties being $\pm 3\%$ in the calorimeter energy [86] and $\pm 5\%$ in the electron-photon transport calculation [87]. If these independent contributions are added quadratically, an uncertainty of about $\pm 6\%$ is obtained for the internal energy at a given location in the sample. The calculated energy deposition gradients across the 25 μm thick powder layer are small; the peak-to-average ratio amounts to only 1.05 [85, Figure 3]. Judging from these numbers, it appears that the energy state of the sample prior to expansion is defined quite well, compared to the in-pile situation previously described.

With respect to the pressure evaluation two comments are necessary. Firstly, there are non-prototypic pressure sources which might have contributed to the total measured pressure:

- water vapor, or gases absorbed on the fine 2- μm -powder,
and
- extrinsic impurities in the uranium oxide.

The pressure contributions from these sources are unknown, but they could be significant. Secondly, a comment needs to be

made concerning the approximately constant pressures seen in the REBA expansion.

Volume expansion in the REBA experiments amounted to 25 to 75 times the initial volume V_0 , depending on the specific experiment. For such large expansion ratios, noticeable cooling of the liquid phase should occur due to vapor production. This in turn would result in a vapor pressure drop and a non-isobaric expansion of the liquid-vapor mixture. The magnitude of this effect was estimated by calculating the liquid internal energy U_L as a function of the expansion ratio V/V_0 . Figure 14 shows $U_L (V/V_0)$ for initial internal energies U_0 which were deposited in REBA experiments, if a Harwell EOS for UO_2 is used [16].

Quenching of the liquid phase during expansion becomes increasingly severe with increasing initial energy deposition U_0 because the vapor densities increase rapidly with liquid internal energy. The circles in Figure 14 indicate the V/V_0 ratio up to which the expansion was followed in the respective REBA experiment. The pressure ratios of initial to final vapor pressure $p_0/p = p(U_0)/p(U_L)$ are given for these points. The dashed line for $U_0 = 1860$ J/g is obtained when the low vapor pressures of the Harwell EOS (Figure 11, upper curve 16-SST) are replaced by the higher pressures evaluated in the REBA experiments themselves. The two lines for $U_0 = 1860$ can be regarded as reasonable upper and lower bounds for $U_L (V/V_0)$.

Considering the large pressure drop ratios p/p , it

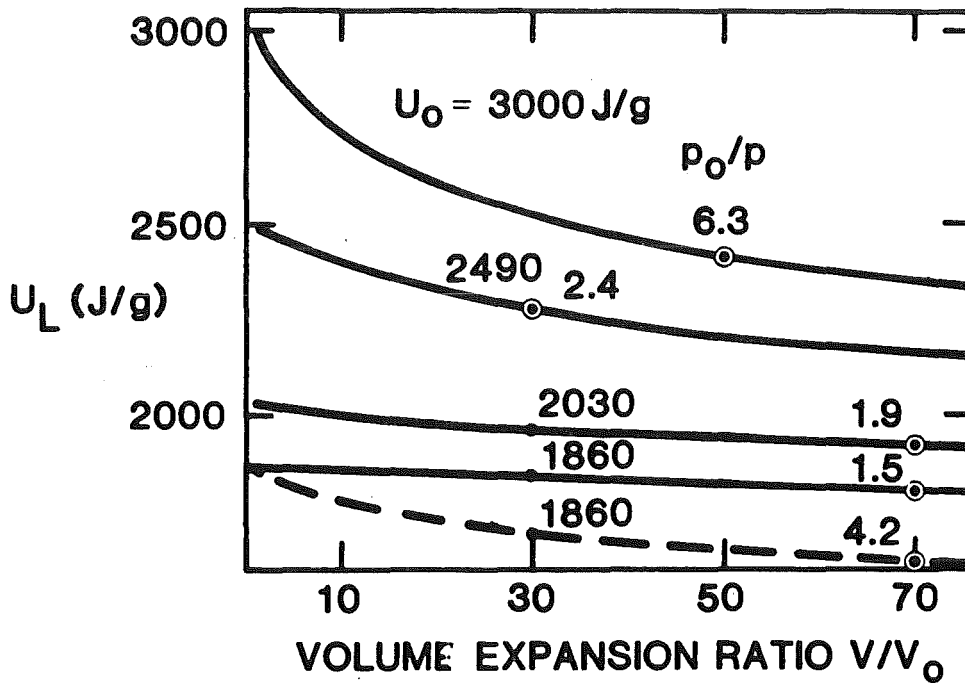


Figure 14. Calculated internal energy of REBA uranium oxide sample during expansion of container volume.

appears that the constant pressures seen in the REBA experiments cannot be due to fuel vapor pressure alone. An additional pressure source, which increased in time, must have balanced the decaying fuel vapor pressure. It should be emphasized that cooling of the liquid oxide during the two-phase expansion is discussed in detail in [85] and used to construct a U-p-V-surface from the REBA pressures. But puzzlingly, it is ignored in deriving the REBA pressures themselves. Since cooling of the liquid UO_2 causes substantial drops in the saturation vapor pressure even at the lowest REBA energy (factor 1.5...4.2), in the author's opinion, the effective REBA pressures cannot be considered pure saturation vapor pressures of $\text{UO}_{2.08}$. Rather the REBA data should be considered an upper pressure bound for $p_{\text{sat}}(\text{U})$ of $\text{UO}_{2.08}$.

It should be added here for clarity that the above mentioned pressure contributions from water vapor, absorbed gases or fuel impurities are not large enough to explain the constant REBA pressures during the expansion. The actual pressure sources in the REBA experiments remain unclear.

4.6 Assessment of p(U) Results

4.6.1 Theoretical Work

Pressure-energy relations for UO_2 were calculated using Corresponding States or Significant Structures Theory [2,14,16]. In both theoretical approaches appreciable uncertainty margins enter from the input data and from the model itself. There is no basis to expect that any of the CST or SST results is

within the goal defined in section 2 ($\pm 6\%$ in U). Since in addition no clear reason exists for preferring one of the curves, one is left with a wide band of possible p-U relations. Only careful measurements can narrow these uncertainties down to the desired level. The dotted curve in Figure 11 is obtained if the IAEA p-T standard from Figure 2 is converted with $c_p = .5 \text{ J/gK}$. This curve should only serve as a temporary reference line between Figures 2 and 11, because the heat capacity of liquid UO_2 is still very uncertain.

4.6.2 Experimental Work

SNL Technique

The measured pressures are likely to be higher than that of pure $\text{UO}_{2.00}$ for two reasons:

- The fuel sample was hyperstoichiometric ($\text{O/U} = 2.08$) and
- Extrinsic contamination was probably introduced during test preparation.

With respect to the energy evaluation, an important open question is that of fuel geometry after melting. If a compacted geometry was attained in the liquid state, the peak energy curves in Figure 11 would have to be shifted to higher energies, into the vicinity of the IAEA reference line.

CEA Technique

The measured pressure can be considered HCDA typical because extrinsic impurities from the test preparation were avoided. With an apparent uncertainty of $\pm 20\%$ the pressure

evaluation is very good. However, the energy evaluation of the boiling fuel zone is much less precise, mainly because energy deposition gradients in the fuel sample and the time dependence of the coupling factor were neglected. A rough estimate for these effects resulted in $16 \pm 3\%$ more energy deposition, thus shifting the CEA data point to about 1900 J/g in Figure 11. Evaluation of the fuel energy with the required precision (± 3 to $\pm 6\%$) remains the main task for the improvement of this promising technique.

SNL Experiment PBE-5S

It should be emphasized that the p-U region shown in Figure 11 does not result from a direct measurement, but from a SIMMER sensitivity study of this integral pin experiment. The uncertainties in the pressure might be quite large. Nevertheless, the analysis seems to indicate a UO_2 vapor pressure close to the IAEA reference line.

REBA Experiments

The energy state of the liquid sample prior to expansion seems to be defined quite well ($\pm 6\%$). With respect to the measured pressures, it was concluded that

- non-prototypical pressure contributions from absorbed water vapor, gases or other extrinsic impurities can be expected,
- the hyperstoichiometric sample composition ($O/U = 2.08$) should result in high pressures compared to $UO_{2.00}$, and

- the isobaric expansion observed in REBA experiments is not compatible with fuel vapor alone, an additional pressure source is needed to explain the isobaric expansion.

Consequently the REBA pressures should be considered upper bounds for the saturation vapor pressure of hyperstoichiometric uranium oxide ($O/U \approx 2.08$). In the author's opinion the saturation vapor pressure of $UO_{2.00}$ is likely to be substantially lower than the REBA data.

As became apparent from the assessment of the REBA results, a number of poorly understood effects exist in this technique. It is unfortunate that this interesting method remained in an experimental stage where it cannot be excluded that unresolved physical mechanisms influenced the taken data.

4.6.3 Summary

The above assessment of the existing p-U work resulted in quite some evidence that the saturation vapor pressure of UO_2 is located in the vicinity of the IAEA reference line. However, this conclusion needs further experimental confirmation.

Comparing the different experimental and theoretical methods, it appears that in-pile EOS experiments provide the most promising approach to the determination of p-U relations of nuclear fuels. The reasons are twofold:

- Heating method and heating time are HCDA typical.

Unknown or not well understood pressure phenomena will

thus be included empirically in the measurements.

- The technique can be extended in a relatively easy way to irradiated (U,Pu) mixed oxide, which is the fuel of ultimate interest for HCDA analyses.

The importance of the last point is obvious. The first point is substantiated by the following examples.

The vapor pressure above a surface increases, according to the Kelvin Equation [94], with decreasing radius of curvature. For UO_2 this effect becomes noticeable with droplets smaller than $.1 \mu m$. On both theoretical and experimental grounds [95], such small particles can be expected during HCDAs, but the overall effect on the vapor pressure is difficult to quantify.

Two more examples for unclear pressure phenomena are the release kinetics for non-fuel species (intrinsic impurities, fission gases) and the pressure interactions between fuel vapor species and non-fuel vapor species. For these reasons, in-pile EOS experiments appear as the most direct and reliable way to the desired p-U information on nuclear fuels.

5. RESULTS FOR (U,Pu) MIXED OXIDES

Although (U,Pu) mixed oxide is the actual Fast Breeder fuel, only little work has been carried out on vapor pressures of (U,Pu) oxides, compared to UO_2 . Theoretical treatments are impeded by the significantly increased complexity of the U-Pu-O system and by the more limited data basis on which a model could be founded. Experimental work is mainly hampered by the excessive technical requirements, associated with handling plutonium bearing fuel. As a result, vapor pressure data for (U,Pu) mixed oxides are scarce and subject to even larger uncertainties than those of UO_2 .

This section summarizes the few published results for fresh and irradiated mixed oxides very briefly. Only the most important new aspects of the methods employed will be discussed.

5.1 Theoretical Results

Gabelnick and Chasanov [28], were the first to estimate the vapor pressure of liquid (U,Pu) mixed oxides, including the pressure contributions from fission products. The mathematical approach is a Law-of-Mass-Action algorithm, based on evaporation equations like Eq. (14). A number of simplifying assumptions are made in the model, the most important ones being uniform temperature, instantaneous chemical equilibrium among elements and oxides, no compound formation between fission products, ideal solution behavior and unhindered access of all vapor species to the free volume. The evaporation equations

are formulated for all fuel vapor species and the most important fission products. This set of equations, which is interconnected by the oxygen partial pressure in the closed system, is then solved iteratively by obeying the additional constraints from mass and volume conservation. The basic parameters in these calculations are temperature, initial fuel composition, burn-up and fuel smear density. In Figure 15, only the results for fresh (U_{.80} Pu_{.20}) O_{1.98} are shown (= oxygen and fuel vapor pressures as taken from the 1% burnup calculation in Ref. 28).

Later, LMA calculations were performed with thermodynamic input data which were felt to be the most probable ones at that time [32]. The resulting most probable saturation vapor pressures are depicted in Figure 15 for three different O/(U+Pu) ratios. Up to 4500 K an uncertainty margin of $\Delta p/p \approx \pm 50\%$ was obtained for the 1- σ band (= 70% confidence interval).

Another theoretical approach which, however, concentrates on the pressure contribution from fission product elements -- excluding any chemistry -- is that of Brook [88]. Using different models for combining vapor pressures, the contributions from fission product elements are combined with the UO₂ vapor pressures of Booth [14].

5.2 Experimental Results

5.2.1 ITU Vacuum Evaporation

The ITU group applied their vacuum evaporation technique also to (U,Pu) mixed oxide [50,89]. The published results are plotted in Figure 15.

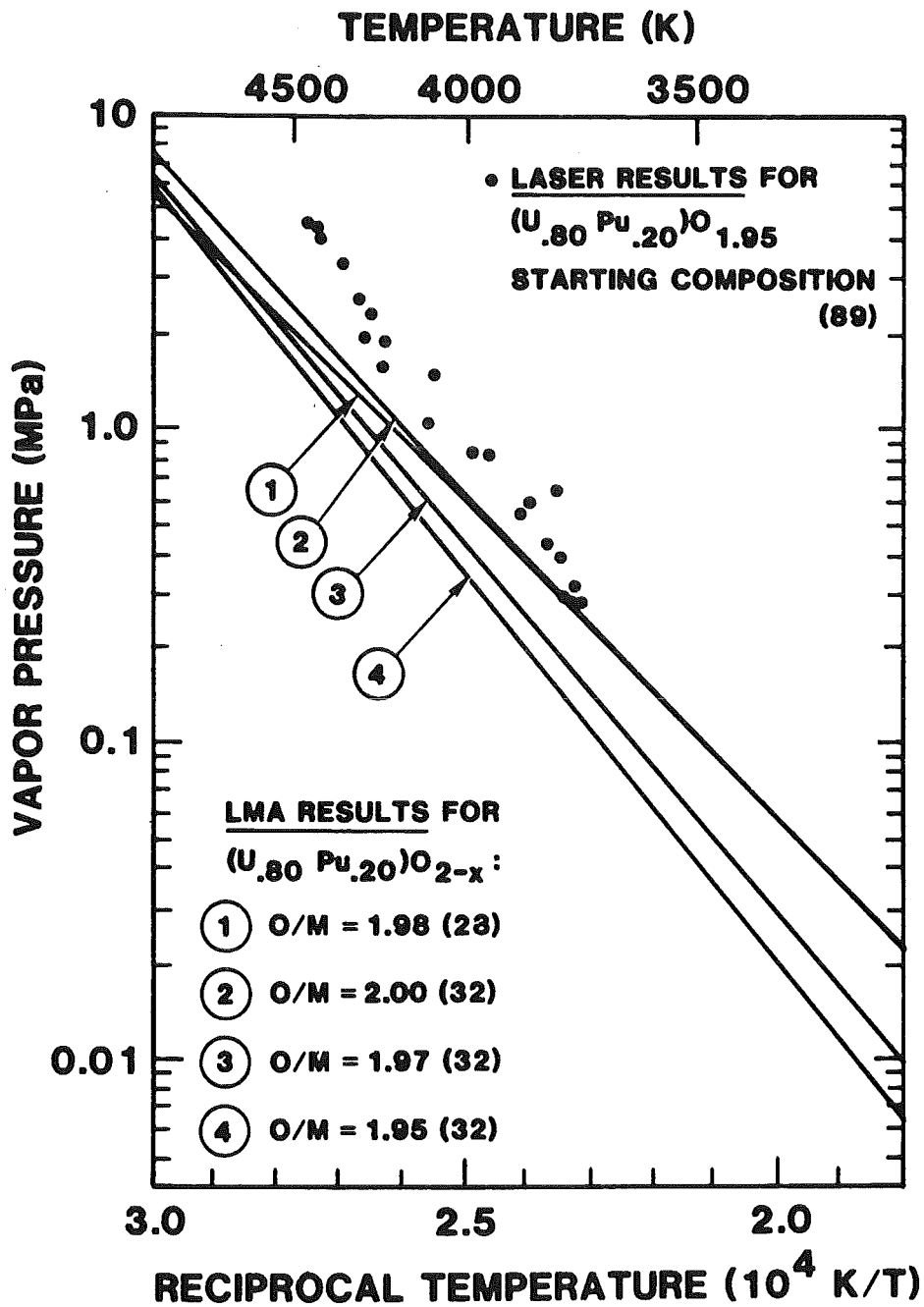


Figure 15. Measured and calculated saturation vapor pressures of liquid (U,Pu) mixed oxide as function of reciprocal temperature.

Aside from the already discussed problems in this technique, two additional ones exist here. Firstly, the emissivity of liquid (U,Pu) mixed oxide is not known in the temperature range of interest. It was originally intended to construct a $\epsilon(\lambda, T)$ surface from pyrometric power density measurements at different wavelength λ_i and different temperatures T_j with the additional assumption that ϵ is a linear function of T [89]. Because no emissivities have been published since, this approach obviously did not lead to satisfactory results. The pyrometer signals in the vapor pressure measurements were evaluated with an emissivity of .80. Equation (25c) predicts that an error of 10% in ϵ would translate into a temperature error of about 1.8%.

The second point is that laser evaporation of mixed oxide must be expected to lead to surface changes not only in the oxygen-to-metal ratio but also in the U-Pu-ratio. The surface composition in the case of mixed oxides is therefore even more uncertain than that of laser heated UO_2 .

5.2.2 VIPER Experiments

An in-pile test program is underway in the British VIPER reactor which aims at identifying amounts and release rates of fission gases from liquid irradiated (U,Pu) mixed oxide [90]. These experiments are specifically directed at the fission gases, excluding pressure contributions from fuel vapor or condensable fission product vapors. So far however, fission gas pressures were dominated by contaminant gases, mainly H_2 , N_2 and CO , and no

definite results are available yet.

5.2.3 SPR III Experiments

A series of experiments was performed in the Sandia Pulsed Reactor (SPR III) in which irradiated mixed oxide samples were heated far into the liquid state in less than 1 ms [91]. The pressures measured in these experiments were surprisingly low. This was rationalized by assuming extreme heat losses during the pressure measuring time due to intensive evaporation - condensation heat transfer. The other conclusion was that fission product release from irradiated fuel takes longer than several milliseconds. In the author's opinion, several problems exist with the experimental technique which make an analysis of the results very difficult:

- Due to high fuel enrichments, large and not well-known energy deposition gradients existed in the fuel samples.
- Fabrication tolerances in the container parts allowed the free volume to change by a factor of 2 during the experiment.
- A large noise signal from the reactor pulse itself seriously disturbed the pressure transducer signal (around -20 MPa in Figure 4 [91]). To correct for this, a scaled fission chamber signal of the reactor pulse was subtracted from the transducer signal. Since this correction procedure is ambiguous and moreover no time separation exists between noise signal and pressure signal, the resulting corrected pressure (+3 MPa in

Figure 4, [91]) is subject to substantial errors.

- Some measured transducer signals decayed in few milliseconds from their peak value directly to negative readings which might have been caused by thermal bowing of the transducer membrane. This possibility is supported by the fact that at low energy depositions where only little liquid or vapor is expected to contact the upper container surface, no such negative pressure excursions were observed.

A test experiment on fresh UO_2 gave about 3 MPa for an energy deposition between 2550 J/g ($=U_{\text{avg}}$) and 2800 J/g ($=U_{\text{pk}}$). (It should be added here for clarity that energies quoted in the Figures of [91] are calculated minimum energies, peak energies are about 50% higher). This result, which contradicts all other U-p data can be taken as an indication for the above discussed experimental problems. In the author's opinion it is highly unlikely that the results obtained for irradiated fuel represent actual mixed oxide vapor pressures.

6. FUTURE RESEARCH NEEDS

In order to bring the still existing, large uncertainties in both p-T and p-U results down to the goals defined in section 2, further research is needed for improving the theoretical and the experimental methods used for the determination of saturation vapor pressures.

6.1 Theoretical Methods

The two theoretical approaches to saturation vapor pressures of UO_2 or $(\text{U,Pu})\text{O}_2$ with the most potential for reaching the goals defined in section 2, seem to be a true Corresponding States Theory and especially the Law-of-Mass-Action.

CST

The main weakness of the Generalized CST approach described in section 3.1 is that little molecular similarity exists between the used reference liquids and UO_2 . Without looking into the detailed problems, the following alternative approach seems more appealing:

1. Determine the molecular nature -- ionic, molecular, metallic -- of liquid UO_2 from experimental or theoretical work,
2. Develop a statistical - mechanical formalism for the " UO_2 -class" on which proper reducing parameters and a universal EOS can be based, and
3. Collect saturation vapor pressure data of class members to construct the dimensionless saturation line of the UO_2 -class.

If liquid UO_2 should be indeed ionic, advantage could be taken of the CST developed for molten salts [92, outlined in 10]. Its molecular reducing parameters are the equivalent hard sphere radius and the ion charge. A convenient set of macroscopic reducing parameters could be the triple point data of the class members, which are much more accessible than critical data. The advantage of such an approach would be, that it is -- as the Simple CST -- again founded on a true Corresponding States formalism.

LMA

The presently existing uncertainties in Law-of-Mass-Action calculations are most effectively reduced by improving the data on those thermodynamic quantities x_i which have either a high weight $\partial p_{\text{sat}}/\partial x_i$ in Equation (19) or a large standard deviation σ_{x_i} .

Most important in the former class are the free enthalpies of formation of liquid UO_2 and gaseous UO_2 , UO_3 and O . Required for the determination of ΔG_f° of these molecules are heat capacities -- especially the electronic contributions in $\text{UO}_2(\text{g})$ and $\text{UO}_3(\text{g})$ -- and the standard quantities ΔH_{298}° and ΔS_{298}° . Low weight, but a large standard deviation exists for the oxygen potential of liquid UO_2 . All data stem from extrapolations of theoretical models into the liquid range, where no experimental data exist. A measurement of the oxygen partial pressure over liquid UO_2 could substantially reduce the uncertainty potential from this source. Oxygen partial pressures could be obtained

with the transpiration method (section 4.1) by analyzing the oxygen content in the carrier gas flow with a solid state oxygen meter. An attractive aspect of such a measurement would be, that it allows to cover both solid and liquid UO_2 , so that the results for liquid UO_2 could be tied to the existing ΔG_{O_2} -models for solid UO_2 .

In summary it appears that the above described research could substantially improve the theoretical basis for saturation vapor pressures of fresh UO_2 or $(\text{U}, \text{Pu})\text{O}_2$. It is highly unlikely, however, that pressure data for irradiated nuclear fuel can be obtained theoretically with the desired precision.

6.2 Experimental Methods

6.2.1 Laser Surface Heating

Before the significance of any laser induced vapor pressure for reactor accident considerations can be assessed, the following important questions must be clarified:

- the optical absorption in the laser induced UO_2 vapor plume,
- the extent of surface composition changes during the experiment and their effect on the measured vapor pressure, and
- the material removal processes in laser induced evaporation.

The question of optical absorption calls for a transmission experiment in which a beam of monochromatic light is sent through a laser produced UO_2 vapor plume and its attenuation

is measured. The path of the probing beam through the non-isothermal vapor cloud should be similar to that taken by thermal radiation in the actual pyrometry.

Surface composition changes could possibly be detected by X-ray diffraction studies on molten crater material, since the lattice parameter of UO_{2-x} depends on x . (Provided oxygen rediffusion during sample cooling is slow enough to freeze the actual surface composition). Also mass spectrometric investigations on the vapor cloud composition could give very valuable information about surface composition changes. Such work is presently underway at LBL [65].

The last of the above three questions probably requires both theoretical and experimental investigations for a proper answer. First the interaction of laser light of power densities between 10^5 and 10^8 W/cm^2 with condensed matter needs to be addressed theoretically. Of main importance are the details of mass transfer at the liquid-vapor interface. Theoretical predictions about the active material removal process should then be tested on materials where the high temperature thermal (phonon driven) evaporation rate is well established. A possible candidate for such a calibration test of laser evaporation could be tungsten around 3000 K. Also mass spectrometric investigations on the vapor composition could reveal important information about the molecular details of laser induced evaporation.

The solution of the above three problems would allow to further develop laser evaporation into a fully approved method

for measuring vapor pressures of refractories or other high temperature materials at temperatures inaccessible to other techniques. With respect to nuclear fuels, the role of laser heating is limited to unirradiated UO_2 and possibly $(\text{U,Pu})\text{O}_2$.

6.2.2 Fission Heating

Both in-pile techniques which have been developed for measuring p-U relations of nuclear fuels require further improvements. The main problem, determination of the fuel energy deposition with a precision between ± 3 and $\pm 6\%$, is a quite demanding task in the hostile reactor environment. Nevertheless, it appears that in-pile experiments are the most promising approach to the desired vapor pressure information for reasons outlined in section 4.6.3. The improvements which were obtained in the SNL technique since the first series [69] are described in [96].

7. SUMMARY

This report represents an attempt to critically review the numerous vapor pressure relations of fresh oxide fuels which have been published during the past 15 years. To allow a clear presentation of this extensive task, the available data base was divided into three sub-areas:

1. theoretical p-T results (Figure 2),
2. experimental p-T results (Figure 4), and
3. theoretical and experimental p-U results (Figure 11).

As a first step in the assessment, the precision was quantified which is required in the fuel saturation vapor pressure data for the purpose of HCDA calculations. It turned out that acceptable pressure uncertainties range between a factor of 2 to 4, which translates into an acceptable uncertainty in the energy variables T and U of only ± 3 to $\pm 6\%$ (Table I). These tolerable uncertainties in p, T and U served as the goals against which the various theoretical and experimental methods were compared. Four theoretical methods for estimating p-T data of liquid UO_2 were investigated (see section 3.5 and Appendix I):

- Corresponding States Theory,
- Significant Structures Theory,
- Law -of-Mass-Action, and the
- Clapeyron Equation.

The assessment indicates that all calculated p-T data are presently afflicted with pressure uncertainty factors greater than 4. In this situation, it appears reasonable to recommend

the IAEA standard because it is close to the mean of all published p-T curves (Fig. 2). The Law-of-Mass-Action approach appears as the most promising theoretical method for reaching the goal of a pressure uncertainty factor below 4 because uncertainties in LMA results come from input data uncertainties only.

Six techniques for measuring p-T data of liquid UO₂ were reviewed (see section 4.3 and Appendix I); namely:

- ANL transpiration technique,
- KfK-INR laser technique,
- LBL-NASA laser techniques,
- two ITU laser techniques, and
- MAP laser technique.

The quite precise transpiration data indicate a saturation vapor pressure slightly below the IAEA standard (Fig. 4). However, since this is not a transient technique, material problems limit the measurements to below 3400 K. Above this temperature only laser results are available. The assessment of pressure and temperature evaluations in these laser techniques led to the conclusion that the combined pressure uncertainty factor is either greater than 4 or close to 4 (KfK-INR technique). However, aside from these experiment-related uncertainties, three basic questions were identified which must be answered before a final assessment of the laser results can be made (section 4.3.6). With these questions unanswered, the measured vapor pressure data above 3400 K remain even more uncertain and their

significance for HCDA calculations -- which require equilibrium data -- is unclear.

The assessment of the published p-U data for liquid UO_2 resulted in the following findings: Calculated p-U relations for UO_2 , using Corresponding States or Significant Structures Theory, scatter widely (Fig. 11) and each curve itself is subject to large uncertainty margins. It appears that only careful measurements can narrow down these uncertainties to the desired level. The assessment of the scattered experimental p-U results showed some evidence that the saturation vapor pressure of UO_2 could be located in the vicinity of the IAEA reference line (Fig. 11). However, this preliminary conclusion needs further experimental confirmation. Most promising experimental approach for locating the p-U curve of UO_2 are in-pile experiments because both, heating method and heating time, are HCDA typical. Also, unknown or not well understood pressure phenomenon would be included empirically (section 4.6.3).

Section 5 summarizes the few published results for fresh and irradiated (U,Pu) mixed oxides. These data are subject to even larger uncertainties than those of UO_2 because of increased difficulties in theoretical and experimental investigations.

Section 6 finally lists the identified areas for which further research is needed in order to bring the large existing uncertainties in both p-T and p-U data down to the desired

factor of 2 to 4 in the saturation vapor pressure (see also Appendix I).

Acknowledgement

The author is indebted to many colleagues at SNL and KfK-INR for stimulating and clarifying discussions, especially to P. Mast and R. W. Ostensen (section 2.1), M. F. Young (section 4.4.3), M. Bober and H. U. Karow (section 4.2.1), and K. A. Long (section 4.3.6.3).

References

1. An excellent summary of HCDA sequences is found in "In-Pile Advanced Reactor Safety Research" by Advanced Reactor Research Department 4420, Sandia National Laboratories, Albuquerque, NM, 87185, USA (October 1977).
2. Jackson, J. F., et al., "An Assessment of the Equation of State in The VENUS-II Disassembly Code", Report ANL/RAS 75-43 (November 1975), Argonne National Laboratory, USA.
3. Refling, J. G., Reynolds, A. B., Garner, P. L., and Rao, S. P., "Nonequilibrium Evaporation and Condensation in Liquid Metal Fast Breeder Reactor Fuel Expansion," Nucl. Technology, 33, 275 (1977).
4. Ostensen, R. W., "A Sensitivity Study on the Damage Potential of a Liquid-Metal Fast Breeder Reactor Core Disassembly", Nuclear Technology, 43, 301 (1979).
5. Buttery, N. E., "The Sensitivity of Excursion Yields to UO_2 Equation of State Uncertainties", Report RD/B/N4623 (1980) Central Electricity Generating Board, Res. Div., Berkeley Nuclear Laboratories, Great Britain.
6. Nicholson, R. B., and Jackson, J. F., "A Sensitivity Study For Fast-Reactor Disassembly Calculations", Report ANL - 7952 (1974), Argonne National Laboratory, USA.
7. Bott, T. F., and Jackson, J. F., "The Influence of Equation-of-State Uncertainties on Fuel Vapor Expansion Work-Energy Calculations," Trans. Amer. Nucl. Soc., 26, 367 (1977).
8. Carter, J. L., and Meyer, J. F., "The Vapor Pressure Equation-of-State in Core Disassembly Calculations," Trans. Amer. Nucl. Soc., 26, 368 (1977).
9. Buttery, N. E., Edwards, A. G., MacInnes, D. A., Findlay, J. R., Wood, M. H. and McTaggart, M. H., "Studies of the Effects of Fuel EOS Uncertainties on FBR Disassembly Energetics," Report SRD R 166 (1979), Safety and Reliability Directorate, UKAEA, Great Britain.
10. Reed, T. M., and Gubbins, K. E., "Applied Statistical Mechanics Thermodynamic and Transport Properties of Fluids," Chapter II, MacGraw Hill, (1973).
11. Hougen, O., Watson, K. M., and Ragatz, R. A.; "Chemical Process Principles" Part II, John Wiley, NY (1959).

12. Meyer, R. A., and Wolfe, B. E.; "High Temperature Equation of State of Uranium Dioxide," Trans. Amer. Nucl. Soc., 7, 111 (1964).
13. Menzies, D. C., "The Equation of State of Uranium Dioxide at High Temperatures and Pressures," UKAEA Report TRG 1119(D) (1966).
14. Booth, D. L., UKAEA Report TRG 1959 (R/X) (1968).
15. Kapil, S. K., "Evaluation of the Thermodynamic Critical Constants for Uranium Dioxide," J. Nucl. Mat., 60, 158, (1976).
16. Browning, P., Gillan, M. J., and Potter, P. E., "The Equation of State of Uranium Dioxide: A Comparison of the Corresponding States and Significant Structures Theories," UKAEA Report AERE-R-8129 (1977).
17. Olander, D. R., "Equation of State of UO_2 ", Chapter 9 in "Fundamental Aspects of Nuclear Reactor Fuel Elements," Report TID-26711-Pl, National Technical Information Service, U.S. Department of Commerce, Springfield, Virginia, 22161, USA.
18. Karow, H.U., unpublished report of the KfK (1979).
19. Eyring, H. and John, M. S., "Significant Liquid Structures," John Wiley, NY, (1969).
20. Gillan, M. J., "Derivation of an Equation of State for Liquid UO_2 Using the Theory of Significant Structures", in "Thermodynamics of Nuclear Materials," IAEA Vienna (1974) p. 270.
21. Fischer, E. A., Kinsman, P. R., and Ohse, R. W., "Critical Assessment of Equation of State Data for UO_2 ," J. Nucl. Mat., 59, 125 (1976).
22. Fischer, E. A., "Equation of State for Substoichiometric Urania Using Significant Structures Theory," in "Thermodynamics of Nuclear Materials 1979", IAEA Vienna (1980) p. 115.
23. Fischer, E. A., and Heger, R., unpublished report of the KfK (1980).

24. Green, D. W., Reedy, G. T., and Leibowitz, L. P., "Thermodynamic Functions and Vapor Pressures of Uranium and Plutonium Oxides at High Temperatures", Seventh Symposium in Thermophysical Properties, A Cezairliyan (Ed.), The Amer. Soc. of Mech. Eng., NY, (1977) 379.
25. Green, D. W., "Calculation of the Thermodynamic Properties of Fuel-Vapor Species from Spectroscopic Data", Report ANL-CEN-RSD-80-2 (1980) Argonne National Laboratory, USA.
26. Ackermann, R. J., Rauh, E. G., and Rand M. H., " A Re-Determination and Re-Assessment of the Thermodynamics of Sublimation of Uranium Dioxide", IAEA - Symposium on Thermodynamics of Nuclear Materials, Jülich; (1977).
27. Rand, M. H. and Markin, T. L., "Some Thermodynamic Aspects of (U,Pu)O₂ Solid Solutions and Their Use as Nuclear Fuels," UKAEA Report AERE-R5560 (1967), Harwell, Great Britain.
28. Gabelnick, S. D. and Chasanov, M. G., "A Computational Approach to the Estimation of Fuel and Fission-Product Vapor Pressures and Oxidation States to 6000 K," Report ANL-7867 (1972), Argonne National Laboratory, USA.
29. Chasanov, M. G., Leibowitz, L. and Gabelnick, S. D., "High Temperature Physical Properties of Fast Reactor Materials," J. Nucl. Mat., 49, 129 (1973/74).
30. Gabelnick, S. D., "Equation of State of UO₂," p. 74 in Chemical Engineering Division, Annual Report, July 1973-June 1974, Report ANL-8120.
31. Breitung, W., "Berechnung der Dampfdrücke von oxidischen Brennstoffen bis 5000 K bei Gleichgewichts - und Nichtgleichgewichts Verdampfung," Report KfK-2091 (1975), Nuclear Research Center Karlsruhe (KfK)
32. Bober, M., Breitung, W., and Karow, H. U., "Thermodynamic Calculation and Experimental Determination of the Equation of State of Oxide Fuels up to 5000 K," Report KfK-2689 (1978), Nuclear Research Center Karlsruhe, (KfK)
33. Finn, P. A., Sheth, A. and Leibowitz, L., "Equation of State of Uranium Dioxide," J. Nucl. Mat., 79, 14 (1979).
34. Long, K. A., Babelot, J.-F., Magill, J., Ohse, R. W., and Hoch, M., "Consistency of Measurements and Calculations of the Total Pressure over UO₂ at High Temperatures: Review of the Specific Heat," High Temperatures-High Pressures, 12, 515 (1980).

35. International Working Group on Fast Reactors, Specialists' Meeting on "Equation of State of Materials of Relevance to the Analysis of Hypothetical Fast Breeder Reactor Accidents," AERE Harwell, U.K., June 1978, Report IWGFR/26, IAEA, Vienna.
36. Johnson, J. D., "Electronic Model for Gaseous UO_2 and the Effect on the UO_2 EOS," p. 88 in Nuclear Reactor Safety Quarterly Progress Report, April 11-June 30, 1979, Report LA-7968-PR, Los Alamos National Scientific Laboratory, Los Alamos, New Mexico.
37. LASL Staff, "An Invitation to Participate in the LASL Equation of State Library," Report LASL-79-62, Los Alamos National Scientific Laboratory, New Mexico (1979).
38. Reedy, G. T. and Chasanov, M. G., "Total Pressure of Uranium-Bearing Species over Molten Urania," J. Nucl. Mat., 42, 341 (1972).
39. Merten, U. and Bell, W. E., "The Transpiration Method," The Characterization of High-Temperature Vapors, J. L. Margrave (Ed.), John Wiley & Sons, New York (1967), 91.
40. Bober, M., Karow, H. U., and Schretzmann, K., "Evaporation Experiments to Determine the Vapor Pressure of UO_2 Fuel (3000-5000 K)," Thermodynam. of Nucl. Materials 1974, Vol. I, 295; IAEA Vienna (1975) also: Nucl. Technology, 26, 237 (1975).
41. Bober, M., Breitung, W., Karow, H. U., and Schretzmann, K., "Evaporation Studies of Liquid Oxide Fuel at Very High Temperatures Using Laser Beam Heating," Report KfK-2366 (1976), Nuclear Research Center Karlsruhe (KfK).
42. Bober, M. and Karow, H. U., "Measurements of Spectral Emissivity of UO_2 Above the Melting Point," Proc. Seventh Symp. on Thermophysical Properties, A. Cezairliyan (Ed.), Amer. Soc. of Mech. Eng., New York (1977), 344.
43. Bober, M., Karow, H. U. and Müller, K., "Study of the Spectral Reflectivity and Emissivity of Liquid Ceramics," High Temp.-High Press., 12, 161 (1980).
44. Karow, H. U., private communication, 1981.
45. Tsai, H. C., Covington, A., and Olander, D. R., "Laser Vaporization of UO_2 ," Report LBL-6016, Materials and Molecular Research Division Annual Report 1976, Lawrence Berkeley Laboratory, University of California, Berkeley, California.

46. Tsai, C. H., "The Kinetics of Laser Pulse Vaporization of UO_2 ," p. 51, LBL Materials and Molecular Research Division Progress Report 1977, LBL-10374, Lawrence Berkeley Laboratory, University of California, Berkeley, California.
47. Covington, M. A., Lin, G. N. and Lincoln, K. A., "Free-Jet Expansions from Laser-Vaporized Planar Surfaces," AIAA Journal, 15, 1174 (1977).
48. Tsai, C. H., "The Kinetics of Laser Pulse Vaporization of UO_2 ," p. 50, LBL Materials and Molecular Research Division Progress Report 1978, LBL-10375, Lawrence Berkeley Laboratory, University of California, Berkeley, California.
49. Tsai, C. H., "The Kinetics of Laser Pulse Vaporization of UO_2 ," p. 26, LBL Materials and Molecular Research Division Progress Report 1979, LBL-11030 (December 1979), Lawrence Berkeley Laboratory, University of California, Berkeley, California.
50. Ohse, R. W., Berrie, P. G., Bogensberger, H. G., and Fischer, E. A., "Contribution of Uranium Plutonium Oxide Pressure, and Influence of Radial Fission Product Distributions on Pin Failure of Fast Breeder Fuels Under Accident Conditions," Thermodyn. of Nucl. Materials 1974, Vol. I, 307, IAEA, Vienna (1975).
51. Babelot, J. F., Brumme, G. D., Kinsman, P. R. and Ohse, R. W., "Vapor Pressure Measurement over Liquid UO_2 and $(U,Pu)O_2$ by Laser Surface Heating Up to 5000 K," Atomwirtschaft-Atomtechnik, 12, 387 (1977).
52. Ohse, R. W., Babelot, J. F., Frezzotti, A., Long, K. A. and Magill, J., "Equation of State of Uranium Oxide: Mach Disk Investigation of Transient Laser Induced UO_2 Vaporization Up to 5000 K," High Temperatures-High Pressures, 12, 537 (1980).
53. Ackermann, R. J., Thorn, R. J. and Winslow, G. H., "Some Fundamental Aspects of Vaporization," Chapter 14, The Characterization of High-Temperature Vapors, Margrave, J. L. (Ed.), John Wiley & Sons, New York (1967).
54. Tran Cong, T. and Bird, G. A., "One-Dimensional Outgassing Problem," Phys. Fluids, 21, 327 (1978).
55. Labuntsov, D. A. and Kryukow, A. P., "Analysis of Intensive Evaporation and Condensation," Int. J. Heat Mass Transfer, 22, 989 (1979).

56. Anisimov, S. I., "Vaporization of Metal Absorbing Laser Radiation," Soviet Physics JETP, 27, No. 1, 182 (1968).
57. Ohse, R. W., Babelot, J. F., Cercignani, C., Kinsman, P. R., Long, K. A., Magill, J., and Scotti, A., "Application of Laser Pulse Heating for the Study of High Temperature Vapors, Phase Transitions and Equation of State," 10th Materials Research Symp. on Characterization of High Temperature Vapors and Gases, September 18-22, 1978, Gaithersburg, Maryland.
58. Olstad, R. A. and Olander, D. R., "Evaporation of Solids by Laser Pulses. I. Iron," J. Appl. Phys., 46, 1499 (1975).
59. Magill, J. and Ohse, R. W., "On the Generation of Transient Capillary Waves on the Surface of Laser Irradiated Targets," J. Nucl. Mat., 71, 191 (1977).
60. Magill, J., Ronchi, C., Babelot, J.-F., Long, K. A., and Ohse, R. W., "Analysis of Laser Surface Heating Experiments for the Determination of High Temperature Equation of State of Fast Breeder Fuels," High Temp.-High Pressures, 12, 503 (1980).
61. Ohse, R. W., Berrie, P. G., Brumme, G. D., and Kinsman, P. R., "Advances in Vapor Pressure Studies over Liquid Uranium Plutonium Oxides Up to 5000 K," Plutonium and Other Actinides, 191, H. Blank and R. Lindner (Eds.), North-Holland Publishing Co., Amsterdam (1976).
62. Asami, N., Nishikawa, M. and Taguchi, M., "Experimental Investigation of the Ultra-High Temperature and Pressure State of Uranium Dioxide," Thermodynamics of Nuclear Materials 1974, Vol. I, 287; IAEA Vienna (1975).
63. Tsai, C. H., "Numerical Simulation of Transient, Incongruent Vaporization Induced by High Power Laser," Report LBL-12125 (January 1981), Lawrence Berkeley Laboratory, University of California, Berkeley, California.
64. Tehranian, F., "Gas Dynamic Model for Laser Induced Evaporation," LBL Materials and Molecular Research Division Progress Report, p39, LBL-11030 (December 1979).
65. Tsai, C. H., "The Kinetics of Laser Pulse Vaporization of UO_2 ," LBL Materials and Molecular Research Division Progress Report 1980, 20, Report LBL-12548 (January 1981).
66. Lincoln, K. A. and Covington, M. A., "Dynamic Sampling of Laser-Induced Vapor Plumes by Mass Spectrometry," Int. J. Mass Spectr. and Ion Phys., 16, 191 (1975).

67. Breitung, W., "Evaporation Kinetics of Oxide Fuels and Their Effect on the Actinide Redistribution in Reactor Fuel Pins and on Fuel Vapor Pressure under Accident Conditions," Report KfK-2240 (1976) (in German), or Report EURFNR-1370 (in English), ERDA Technical Information Center, Oak Ridge, Tennessee.
68. D. R. Olander, private communication.
69. Olstad, R. A. and Olander, D. R., "Evaporation of Solids by Laser Pulses. II. Zirconium Hydride," J. Appl. Phys., 46, 1509 (1975).
70. Long, K. A., private communication.
71. Reil, K. O., "Effective Equation of State Measurements on Uranium Dioxide," Dissertation, Nuclear Engineering Department, University of New Mexico, Albuquerque, New Mexico (1977).
72. Reil, K. O. and Cronenberg, A. W., "Effective Equation-of-State Measurements on Uranium Dioxide," Trans. of the Amer. Nucl. Soc., 27, 576 (1977).
73. Breitung, W., Gorham-Bergeron, E., and Murata, K. K., "Analysis of Sandia In-Pile EOS Experiments," Proc. Intern. Meeting on Fast Breeder Reactor Safety Technology, August 19-23, 1979, Seattle, Washington, Vol. II, p. 1059.
74. Murata, K. K., private communication.
75. Murata, K. K., private communication, January 1980.
76. Breitung, W., "Investigation of the Importance of CO Formation in Sandia In-Pile EOS Experiments," Advanced Reactor Safety Research Report October 1978-March 1979, p. 74, Report SAND79-1566 (August 1980), Sandia National Laboratories, Albuquerque, New Mexico.
77. Breitung, W., Murata, K. K., Reil, O. K. and Schumacher, G., "Joint In-Pile Equation of State Series on Nuclear Fuels at Sandia National Laboratories," p. 9, Report SAND80-1794, Sandia National Laboratories, Albuquerque, New Mexico (November 1980).
78. Breitung, W., "Contamination Control in Sandia Equation-of-State Experiments," Report SAND80-1277, Sandia National Laboratories, Albuquerque, New Mexico (October 1980).

79. Combette, P., Barthelemy, P., Manaranche, J. C., and Barbry, F., "Equation of State for LMFBR Fuel (Measurement of Fission Gas Release During Transients)," Vol. II, p. 1052, Proc. Intern. Meeting on Fast Reactor Safety Technology, August 19-23, 1979, Seattle, Washington.
80. Breitung, W., "In-Pile Calorimetry in the Joint Sandia/KfK Equation-of-State Experiments on Nuclear Fuels," Report SAND80-2575, Sandia National Laboratories, Albuquerque, New Mexico (February 1981).
81. Reil, K. O. and Young, M. F., "Prompt Burst Energetics Experiments: Fresh Oxide/Sodium Series," Report SAND78-1561, Sandia National Laboratories, Albuquerque, New Mexico (August 1978).
82. Dickerman, C. E., Robinson, L. E., Agraval, A. K., Murphy, W. F. and Wright, A. E., "Initial TREAT Loop Experiments on LMFBR Oxide Fuel Behavior During A Power Excursion (Tests E1 and E2)," Report ANL-8099, Argonne National Laboratory, Argonne, Illinois (May 1974).
83. Doerner, R. C., Rothman, A. B., DeVolpi, A., Dickerman, C. E., Deitrich, L. W., Stahl, D. and Murphy, W. F., "Final Summary Report on Fuel Dynamics Tests H2 and E4," Report ANL-RAS 74-28, Argonne National Laboratory, Argonne, Illinois (September 1974).
84. Hitchcock, J. T., "SIMMER Analysis of Prompt Burst Energetics Experiments," Report SAND81-0933, Sandia National Laboratories, Albuquerque, New Mexico (1981).
85. Benson, D. A., "Application of Pulsed Electron Beam Vaporization to Studies of UO_2 ," Report SAND77-0429, Sandia National Laboratories, Albuquerque, New Mexico (June 1977).
86. Benson, D. A. and Ouellette, "Fast Rise Time Calorimeter for Relativistic Electron Beam Diagnostics," Rev. Sci. Instrum., 47, 291 (1976).
87. Lockwood, G. J., Halbleib, J. A. and Miller, G. H., "Electron Transport in Reactor Materials," IEEE Trans. on Nucl. Sci., 25, 1581 (1978).
88. Brook, A. J., "Some Preliminary Considerations Relating to An Equation of State for Irradiated Nuclear Fuel," Report SRD-R-13 (1972), Safety and Reliability Directorate, Arlcheth, Warrington, U.K.

89. Ohse, R. W., Berrie, P. G., Brumme, G. D. and Kinsman, P. R., "Advances in Vapor Pressure Studies over Liquid Uranium Plutonium Oxides up to 5000 K," Plutonium and Other Actinides, 91, H. Blank and R. Lindner (Eds.), North-Holland Publishing Co., Amsterdam, Netherlands (1976).
90. McTaggart, M. H. and Findlay, J. R., "Progress Report on the VIPER Measurements of Fission Product Pressure Generation October 1978 to March 1979," Report SRD R 161, private communication.
91. Benson, D. A. and Gorham-Bergeron, E., "Fission Product Release From Dynamically Heated Mixed Oxide Reactor Fuels," High Temp. Sci., 13 21 (1981).
92. Reiss, H., Mayer, S. W. and Katz, J. L., "Law of Corresponding States for Fused Salts," J. Chem. Phys., 35, 820 (1961).
93. Combette, P., private communication.
94. Adamson, A. W., Physical Chemistry of Surfaces, John Wiley and Sons, Inc., NY, (1976), p. 51.
95. Elrick, R. M., "Kinetics of Fission-Vaporized UO₂ Fuel Determined from Sampled Fuel Debris," Proc. Int. Meeting on Fast Breeder Reactor Safety Technology, August 19-23, 1979, Seattle, WA, Vol. II, p. 1043.
96. Reil, K. O., Breitung, W. and Murata, K. K., "Total Vapor Pressure Measurements on Nuclear Fuel Using Fission Heating," Proc. of the 8th Symposium on Thermophysical Properties, National Bureau of Standards, Gaithersburg, MD, USA, June 15-18, 1981.
97. Ohse, R. W. and Kinsman, P. R., "Study of the Equation of State of Uranium Plutonium Oxide Fuels up to 5000k by a New High-Temperature Laser Technique," High Temperatures-High Pressures, 8, 209 (1976).

APPENDIX I: Viewgraph Summary

1. Theoretical methods for predicting p-T data
 - 1.1 Corresponding States Theory
 - 1.2 Significant Structure Theory
 - 1.3 Law of Mass Action

2. Experimental techniques for measuring p-T data
 - 2.1 ANL transpiration technique
 - 2.2 KfK-INR laser technique
 - 2.3 LBL-NASA laser technique
 - 2.4 ITU laser technique (vacuum evaporation)
 - 2.5 ITU laser technique (mach-disk)

3. Experimental techniques for measuring p-U data
 - 3.1 SNL fission heating
 - 3.2 CEA fission heating
 - 3.3 SNL electron beam heating

4. Research needs
 - 4.1 p-T calculations
 - 4.2 p-T laser measurements
 - 4.3 p-U measurements

1.1

CST: UNCERTAINTIES IN CALCULATED PRESSURES RESULT FROM
INPUT DATA AND MODEL ITSELF, MAKING $P/P_0 > 4$

$$P_R = F(T_R, V_R, Z_C) \quad Z_C = \frac{P_C V_C}{RT_C}$$

- CRITICAL DATA OF UO_2 VERY UNCERTAIN ($T_C = 6000 \dots 10000$ K)
- GENERALIZED CST EMPIRICAL IN NATURE
- POOR MOLECULAR SIMILARITY WITH REFERENCE LIQUIDS
 - LIQUID UO_2 IONIC (?)
 - THERMAL IONIZATION DISTORTS MOLECULAR POTENTIALS
 - INCONGRUENT VAPORIZATION: $UO_2(\ell) \rightarrow U, UO, UO_2, UO_3, O, O_2$

1.2

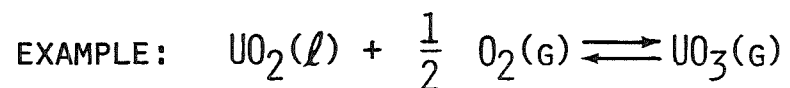
SST: UNCERTAINTIES IN CALCULATED PRESSURES RESULT FROM
INPUT DATA AND MODEL ITSELF, MAKING $P/P_0 > 4$

$$Z_l(V,T) = Z_s^{NV_s/V} \cdot Z_g^{N(V-V_s)/V} \quad Z_l \rightarrow P_{SAT}$$

- P_{SAT} IS HIGHLY SENSITIVE TO INPUT DATA
 - FACTOR 6 FROM VARIATION IN Z_s DATA
 - FACTOR 8 FROM VARIATION IN Z_g DATA
- SST IS A SEMI-EMPIRICAL APPROACH
 - STARTS FROM MOLECULAR PROPERTIES
 - INTUITIVE PARTITION FUNCTION FOR LIQUID

1.3

LMA: UNCERTAINTIES IN CALCULATED PRESSURES RESULT FROM
INPUT DATA ONLY; BUT STILL LARGE, MAKING $P/P_0 > 4$



$$P_{UO_3} = \text{EXP} \left\{ \frac{\Delta G_F^\circ [UO_2(\ell)] + \frac{1}{2} \Delta \bar{G}_{O_2} - \Delta G_F^\circ [UO_3(g)]}{RT} \right\}$$

LMA FULLY DESCRIBES EVAPORATION CHEMISTRY OF CONDENSED UO_2

-- VAPOR SPECIES U, UO, UO_2 , UO_3 , O, O_2

LMA IS A PROVEN PHYSICAL LAW

-- NO EMPIRICAL PARAMETERS

-- UNCERTAINTIES IN ΔG_F° AND $\Delta \bar{G}_{O_2}$ STILL TOO LARGE

2.1

ANL TRANSPIRATION TECHNIQUE: UNCERTAINTIES IN MEASURED

P-T DATA ARE SMALL, MAKING $P/P_0 < 2$; BUT $T < 3400$ K

P: $P_T = P_U (1 + N_C/N_U)$; $\delta P/P = \pm 10\%$

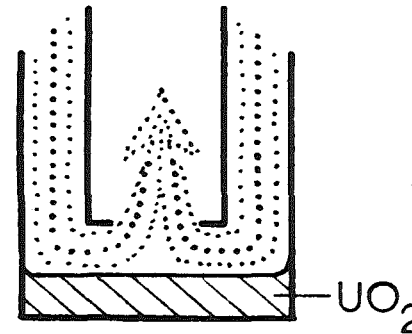
T: OPTICAL PYROMETRY ; $\delta T/T = \pm 1\%$

- METHOD REPRODUCES KNOWN RESULTS FOR SOLID UO_2

- TRUE THERMAL EQUILIBRIUM VAPORIZATION:

LATTICE PHONONS \longrightarrow SURFACE ATOMS \longrightarrow VAPOR ATOMS

- NOT A TRANSIENT METHOD, $T < 3400$ K



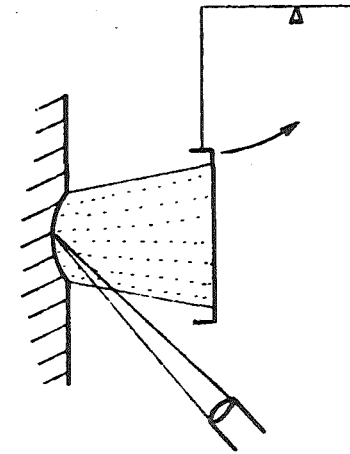
2.2

KFK-INR LASER TECHNIQUE: THE ACHIEVED UNCERTAINTY

LEVEL CORRESPONDS TO $P/P_0 \approx 4$

P: VAPOR PROPERTIES AT PENDULUM
↓
GAS DYNAMIC MODEL FOR VAPOR PLUME
↓
VAPOR PRESSURE AT SURFACE, $P/P_0 = 3 (M+D)$

T: A) FROM GAS DYNAMIC MODEL, $\delta T/T = \pm 6\%$
B) FROM OPTICAL PYROMETRY, $\delta T/T = \pm 1\%$
ε MEASURED



- VALID APPROACH FOR MEASURING LASER INDUCED $P_{SAT}(T)$ OF UO_{2-x} , BUT
 - IS P AN EQUILIBRIUM QUANTITY?
 - WHAT ARE THE EFFECTS OF SURFACE CHANGES ON MEASURED P?
 - IS LIGHT ABSORPTION IN UO_2 VAPOR REALLY NEGLIGIBLE?

2.3

LBL-NASA LASER TECHNIQUE: NO EVALUATION SEEMS
POSSIBLE DUE TO UNRESOLVED PRESSURE UNCERTAINTIES

P: FROM MACH-DISK RELATION FOR RES. EXP.

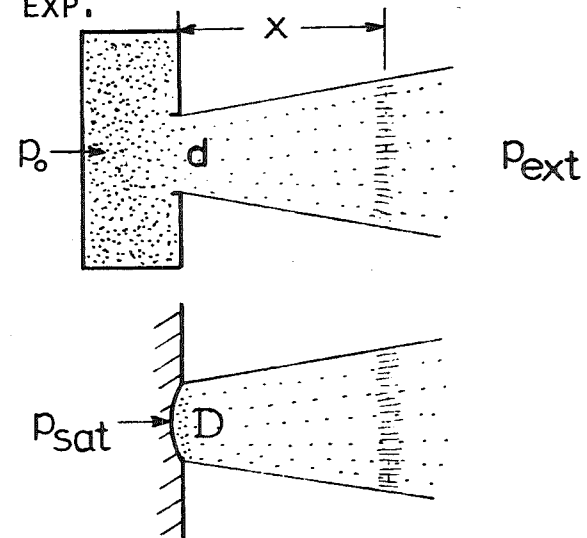
$$P_0 = \frac{P_{EXT}}{C^2} \left(\frac{x}{D}\right)^2$$

AND THE ANALOGY

$$P_0 \hat{=} P_{SAT}(R=0) \quad ; \quad D \hat{=} D$$

T: WIDE BAND SILICON PHOTODETECTOR

- SURPRISINGLY LOW P_{SAT} FOR UO_2
- ANALOGY NEEDS FURTHER THEORETICAL FOUNDATIONS



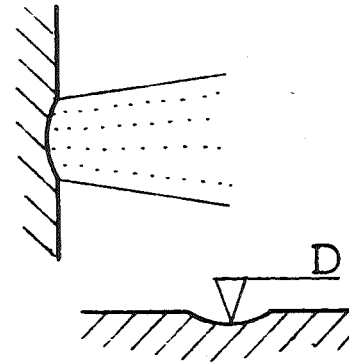
2.4

ITU LASER TECHNIQUE (VAC. EVAP.): NO EVALUATION SEEMS
POSSIBLE DUE TO UNRESOLVED PRESSURE UNCERTAINTIES

P: FROM HERTZ-KNUDSEN EQUATION

$$\frac{1}{A} \cdot \frac{DM}{DT} = \alpha_V \cdot P_{SAT} (M/2\pi RT)^{1/2}$$

↑
FROM CENTRAL CRATER DEPTH D



T: OPTICAL PYROMETRY WITH $\epsilon = .84$

$$(\delta T/T)_{SYST} = -1.4 \dots 2.9\%, (\delta T/T)_{RAND} = \pm 1\%$$

- PRESSURE EVALUATION MODEL HAS LITTLE PHYSICAL RELEVANCE
TO LASER CONDITIONS - H.K. EQ. BASED ON UNPROVEN ASSUMPTION
 - ALL DEVIATIONS LUMPED INTO EMPIRICAL α_V (+ PHYSICS)
 - EMPIRICAL α_V UNKNOWN (.1 TO 1, 2, 3, ...)

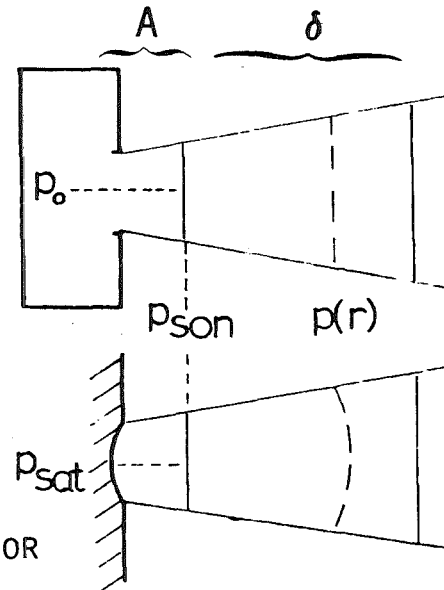


2.5

ITU MACH-DISK VARIATION: ENLARGES THEORETICAL BASIS, BUT
UNRESOLVED PRESSURE UNCERTAINTIES REMAIN

$$P_{SAT} = [M.D.] \cdot \frac{1}{A\delta^2}$$

- P_{SAT} DOMINATED BY NEW FACTOR (~ 10)
- ADIABATIC, MONATOMIC CALCULATIONS
IGNORE UO_2 VAPOR PROPERTIES:
 - MULTICOMPONENT MIXTURE
 - INTERNAL DEGREES OF FREEDOM
 - CONDENSATION OF SUPERSATURATED UO_2 VAPOR
- INFLUENCE OF THESE EFFECTS ON A , δ NEED TO BE INVESTIGATED
BEFORE PRESSURE UNCERTAINTIES CAN BE ASSESSED



3.1

SNL FISSION HEATING: SIGNIFICANT UNCERTAINTY MARGINS
RESULT MAINLY FROM ENERGY EVALUATION; MAKING $p/p_0 > 4$

P: PR. TRANSDUCER MONITORS $p(t)$ IN CLOSED VOLUME

-- IMPURITIES LIKELY

(1 FINGERPRINT TOO MUCH)

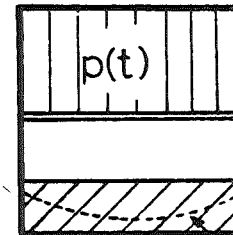
-- $UO_{2.08}$

U: CORRESPONDING $U(t)$ CALCULATED

-- $U(\vec{r})$ DUE TO SELF SHIELDING

-- $U(t)$ DUE TO $p(t)$ AND CHANGING FUEL GEOMETRY

-- UPPER AND LOWER BOUNDS $U_{PK}(t)$ AND $U_{AVG}(t)$



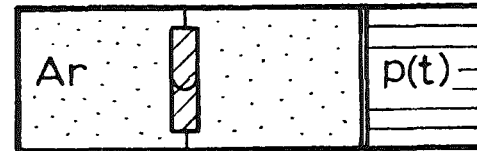
- U_{PK} DEPENDS STRONGLY ON MOVEMENT OF FUEL IN LIQUID STATE
(DISPERSED OR COMPACTED?)

UPPER BOUND UNCERTAIN

3.2

CEA FISSION HEATING: THE PRECISE PRESSURE MEASUREMENT
IS SPOILED BY AN INCOMPLETE ENERGY EVALUATION, MAKING $P/P_0 > 4$

P: CHANGE IN SLOPE OF $P(T)$ INDICATES
BOILING ONSET: $P_{SAT} = P_{AR}$
 $\delta P/P = \pm 10\%$



U: ONLY AVERAGE FUEL ENERGY IS EVALUATED, NEEDED IS $U(\bar{r}_{BOIL}, T_{BOIL})$
NEGLECTED ARE -- ENERGY DEPOSITION GRADIENTS
-- TIME DEPENDENT COUPLING FACTOR (W/G/MW)

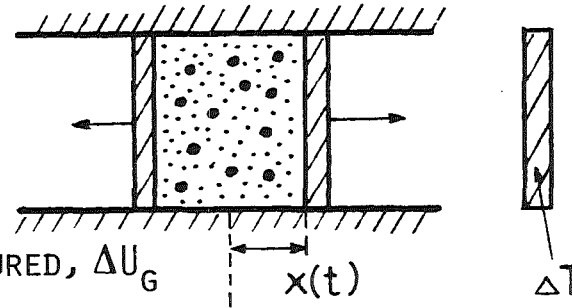
- VERY PRECISE EVALUATION, CONTAMINATION CONTROLLED
- CEA AVERAGE ENERGY $16 \pm 3\%$ BELOW ACTUAL $U(\bar{r}_{BOIL}, T_{BOIL})$

3.3

SNL ELECTRON BEAM HEATING: THE RESULTS ARE UPPER PRESSURE BOUNDS FOR P_{SAT} OF $UO_{2.08}$, SUBSTANTIALLY ABOVE PURE UO_2 PRESSURES

P: FROM MEASURED $x(t)$ AND EQ.

OF MOTION
$$P = \frac{M}{A} \cdot \ddot{x}$$

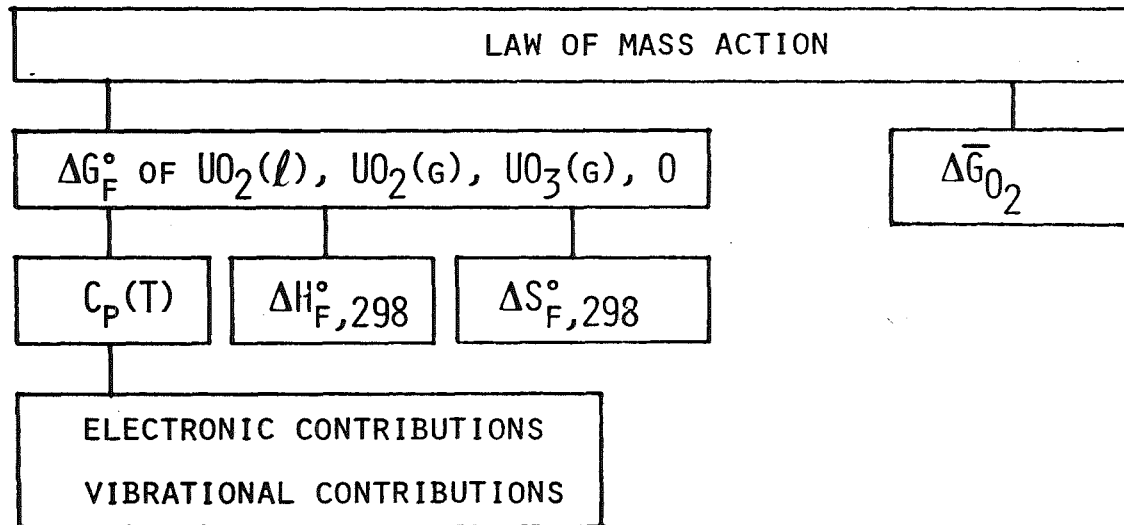


U: 1. ΔT OF GRAPHITE DOSIM. MEASURED, ΔU_G
 2. EXTRAPOLATED TO SAMPLE WITH ELECTRON TRANSPORT CODE; $\delta U/U = \pm 6\%$

- OBSERVED ISOBARIC EXPANSIONS ARE NOT COMPATIBLE WITH PURE FUEL VAPORIZATION (VAP. \rightarrow LIQ. COOLING \rightarrow PRESSURE DROP) ADDITIONAL PRESSURE SOURCE NEEDED
- PROBABLE CONTRIBUTIONS: ADSORB. H_2O , GASES, FUEL IMPURITIES ($2\mu m$)

4.1

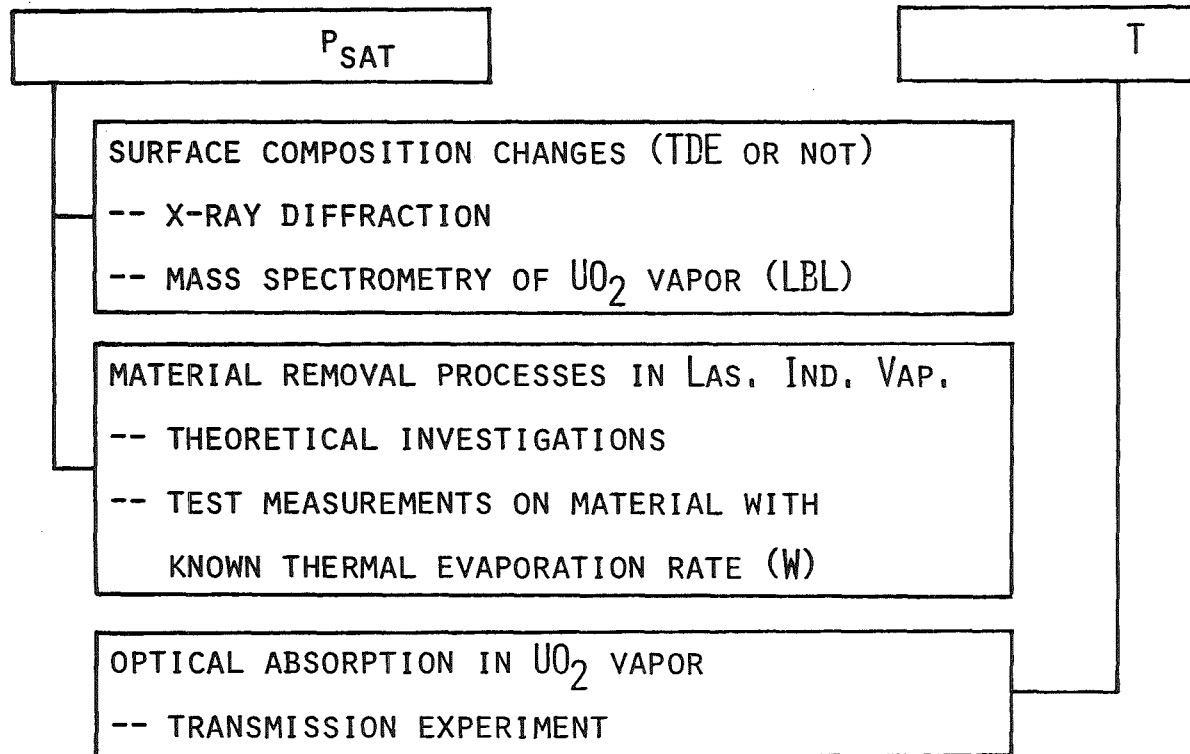
RESEARCH IS NEEDED FOR P-T CALCULATIONS



• EXPERIMENTAL DATA AND THEORETICAL MODELS REQUIRED

4.2

RESEARCH IS NEEDED FOR UNDERSTANDING SIGNIFICANCE
OF P-T LASER RESULTS



4.3

RESEARCH IS NEEDED FOR P-U MEASUREMENTS

